# Evaluation of Battery Performance in MMC based BESS

by

Ishaan Puranik

A Thesis Presented in Partial Fulfillment
of the Requirements for the Degree
Master of Science

Approved April 2018 by the
Graduate Supervisory Committee

Jiangchao Qin, Chair
George Karady
Hongbin Yu

ARIZONA STATE UNIVERSITY
May 2018

ABSTRACT

Li-ion batteries are being used on a large scale varying from consumer electronics to electric vehicles. The key to efficient use of batteries is implementing a well-developed battery management system. It is imperative to develop Li-ion cell model that replicate the performance of a physical cell unit. This report discusses a dual polarization cell model and a battery management system implemented to control the operation of the battery. The Li-ion cell is modelled, and the performance is observed in PLECS environment.

The main aspect of this report studies the viability of Li-ion battery application in Battery Energy Storage System (BESS) in Modular multilevel converter (MMC). MMC-based BESS is a promising solution for grid-level battery energy storage to accelerate utilization and integration of intermittent renewable energy resources, i.e., solar and wind energy. When the battery units are directly integrated in submodules (SMs) without dc-dc interfaced converters, this configuration provides highest system efficiency and lowest cost. However, the lifetime of battery will be affected by the low-frequency components contained in charging and discharging currents, i.e., arm-currents, which has not been thoroughly investigated. This paper investigates impact of various low-frequency arm-current ripples on lifetime of Li-ion battery cells and evaluate performance of battery charging and discharging in an MMC-BESS without dc-dc interfaced converters.

*Nomenclature: Battery Management System (BMS), Lithium Ion (Li-ion), Electric Vehicles (EV), Hybrid Electric Vehicles (HEV), Dual Polarization model (DP model), State of Charge (SoC), State of Health (SoH), Open Circuit Voltage (OCV), Multilevel Modular Converter (MMC), Battery Energy Storage System (BESS)*

*Note: In this paper, the term cell and battery have been used interchangeably as the performance of the cell can be extended to the battery unit.*

ACKNOWLEDGMENTS

I would firstly like to acknowledge and thank my advisor and guide Prof. Dr. Jingchao Qin. His unwavering support, guidance and interest throughout this project has made this project a success.

Secondly, I would like to express my gratitude and special thanks towards Lei Zhang for his continuous support and guidance throughout my project. Lei's encouragement and belief in what he does has been my constant source of inspiration.

I would also like to thank my friends who have become my family in this new journey and who have constantly supported me through thick and thin.

Last but not least, I would like to thank my parents. They have continuously believed in me and always provided me with the resources and opportunities which helped me in achieving my dreams and aspirations.

TABLE OF CONTENTS

Page

CHAPTER Page

CHAPTER Page

LIST OF TABLES

Table Page

LIST OF FIGURES

Figure Page

Figure Page

# I. INTRODUCTION

Batteries are the power house of large number of appliances/EV's in today's world where compactness is of great value. Making the device compact calls for compact batteries as well with a drawback of inefficient cooling. Also, these applications call for maximum run time (capacity) of the batteries. Thus, low power dissipation and higher capacity of the battery are the properties of prime importance. This can be achieved by implementing a well-developed BMS. Having an accurate battery model on hand, we can predict and optimize the performance of the battery.

In this paper, an electrical equivalent model of Li-ion battery is discussed. The model known as Thevenin equivalent model or duel polarization model is considered. The reason to consider Li-ion batteries for the study lies in the fact that it is the most widely used type in electronic applications and EV's. Lithium is the lightest metal on earth and is very highly chemically unstable. Lithium metal ore can be used to fabricate batteries with high energy to weight ratio. Moreover, Li-ion batteries have further advantages like low stand by losses, longer cycle based life and no memory effect.

In this report, we shall discuss the details of the battery model and then will further implement BMS. BMS is a crucial part for efficient performance of the battery. From many studies, it has come to light that it is because of the BMS used by Tesla, their Li-ion batteries over perform. The BMS will take into effect the change in physical environmental conditions like temperature and electrical quantities to optimize the battery performance.

Renewable energy sources are widely integrated into power grids during recent decades, i.e., solar and wind energy resources. To increase penetration of renewable energy resources, the battery energy storage systems (BESSs) need to be deployed and installed to compensate power fluctuations due to intermittent resources. The grid-level BESSs can also provide grid support to improve economy and serviceability. Li-ion batteries due to their high energy density and stability are replacing the traditionally used lead acid batteries in BESSs.

Different converter topologies are employed to implement BESSs, including two-level voltage-sourced converter (VSC) and multilevel converters. Among them, modular-based converters such as modular multilevel converter (MMC) and cascaded H-bridge converter (CHB) are most promising due to their improved performance in reliability, scalability, maintainability, and functionality [1] [2] [3]. The MMC-based BESS (MMC-BESS) can also provide a medium/high-voltage dc link to interface dc grid. The small battery units are integrated into submodules (SMs) with or without dc-dc converters.

For the configuration without dc-dc converters, it provides the highest efficiency and lowest cost. However, large amount of low-frequency components in arm currents to charge and discharge the batteries may seriously affect lifetime of battery. However, the influence of low-frequency current ripple might not be linearly proportional to the percentage of current ripple. This can be used for designing dc-side filter of each submodule in MMC. For instance, if designed so that the current ripple is fully absorbed by active power decoupling circuits, it is not cost effective. If current ripple is fully

absorbed by battery unit, it might severely influence battery lifetime. In this way, the trade-off between filter design and battery lifetime should be considered.

Therefore, this study will investigate impact of low-frequency arm-current ripple on lifetime of Li-ion battery for MMC-based BESS applications based on analytical and experimental studies.

## II. LITHIUM-ION BATTERIES

Li-ion batteries have proven to be superior over the other cell chemistries like NiMH, NiCd or long used Lead acid batteries due to advantages like very high specific energy due to high nominal voltage rating of 3.6V and flat discharge voltage curve though range of 2.8V to 3.7V. Due to this Li-ion cells are most widely used today ranging from low power applications like consumer electronics to medium power applications like electric vehicles and have even penetrated high power applications for battery energy storage systems in transmission and distribution sector.

Advantages of Li-ion batteries:

1. Long cycle life.
2. No maintenance is required during its lifetime.
3. Low self-discharge and hence have long shelf life.
4. High capacity.
5. Low internal resistance.
6. Good coulombic efficiency.
7. Simple charging algorithm.
8. Fast charging.

Disadvantages of Li-ion batteries:

1. Protection circuit is required to prevent over heating leading to thermal runaway.
2. Fast degradation at high operating temperatures.
3. Slow charging at temperatures below $0^0$C.

A. Composition and Working:

Li-ion batteries consists of a Cathode (positive electrode) made of Lithium metal oxide and the anode (negative electrode) of porous carbon usually graphite. Graphite gives the Li-ion batteries the characteristic flat discharge curve. During the charging process, the ions flow from the cathode to the anode through the electrolyte. While the flow direction is reversed for discharge process. For the discharge process, the anode undergoes oxidization, i.e. loss of electrons and cathode undergoes reduction reaction i.e. gain of electrons. The opposite occurs during the charging process. Figure 1 indicates the flow of electrons in the cell:

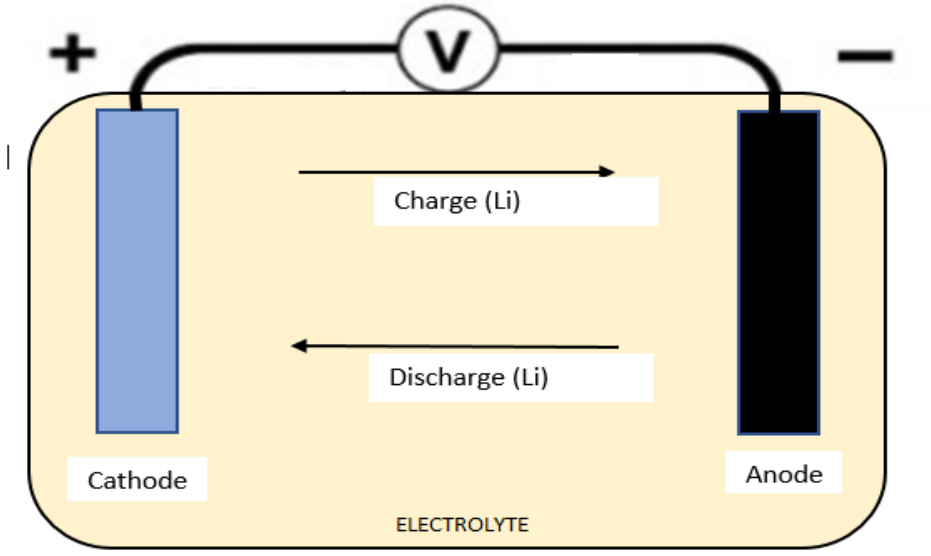


Figure 1. Li-ion battery working.

Current Li-ion cells consist of graphite anode lightly doped with silicon on a copper current collector, Li-oxide cathode coated on Aluminum current collector. The electrolyte is usually an organic solvent diffused with Lithium salt.

B. Types of Li-Ion Batteries:

Table 1 summarizes different types Li-ion battery technologies [10]

| **Type of Battery** | **Lithium Cobalt Oxide** | **Lithium Manganese Oxide** | **Lithium Nickel Manganese** | **Lithium Iron Phosphate** | **Lithium Nickel Cobalt Aluminum Oxide** | **Lithium Titanite** |
|---|---|---|---|---|---|---|
| Symbolic Name | $LiCoC_2$ (LCO) | $LiMn_2O_4$ (LMO) | $LiNiMnCoO_2$ (NMC) | $LiFePo_4$ (LFP) | $LiNiCoAlO_2$ (NCA) | $Li_2TiO_3$ (LTO) |
| Nominal voltage | 3.60V | 3.70V (3.80V) | 3.60V (3.70V) | 3.20, 3.30V | 3.60V | 2.40V |
| Charge Termination Voltage | 4.20V | 4.20V | 4.20V (or higher) | 3.65V | 4.20V | 2.85V |
| Discharge cut-off voltage | 3.00V | 3.00V | 3.00V | 2.50V | 3.00V | 1.80V |
| Specific Energy | 150–200Wh/kg | 100–150Wh/kg | 150–220Wh/kg | 90–120Wh/kg | 200-260Wh/kg | 70–80Wh/kg |
| Safe Charge rate | 0.7–1C (3h) | 0.7–1C (3h) | 0.7–1C (3h) | 1C (3h) | 1C | 1C (5C max) |
| Safe Discharge rate | 1C (1h) | 1C, 10C possible | 1–2C | 1C (25C pule) | 1C | 10C possible |
| Cycle life (Ideal) | 500–1000 | 300–700 | 1000–2000 | 1000–2000 | 500 | 3,000–7,000 |
| Thermal runaway | 150°C (higher when empty) | 250°C (higher when empty) | 210°C (higher when empty) | 270°C (safe at full charge) | 150°C (higher when empty) | Extremely Safe |
| Characteristics | High energy, limited power. | High power, less capacity. | High capacity and high power. | Flat discharge voltage, high power | Highest capacity with moderate power. | Long life, fast charge, Low capacity, expensive. |

Table 1. Types of Li-ion battery technologies.

C. NCA Cells

The cell used for test purposes is the Panasonic NCR 18650B. NCR cells are same as NCA cells where N and C stand for Nickle and Cobalt, respectively while A stands for Aluminum and R stands for Rechargeable. In fact, NCA and NCR have same composition i.e. Lithium-Nickle-Cobalt-Aluminum-Oxide ($LiNiCoAlO_2$). $LiNiCoAlO_2$ Panasonic cells have high energy density, negligible decrease in capacity during storage and high safety factor due to integrated PTC resistant material used in it. For these purposes the cell was chosen for testing purposes. The datasheet in Appendix A summarizes the uniqueness of this cell.

The NCA cells are similar to NMC (Nickle-Manganese-Cobalt) cells but have low discharge current capabilities but they make it up with excellent capacity and large cycle life. These cells are resistant to mechanical shocks thus making a viable option for automotive applications. Tesla implements same cells in their vehicles.

## III. LI-ION BATTERY TERMINOLOGIES

All battery terminologies can be applied to the single cell unit.

### A. C-Rate

The C-rate is charging/discharging current which will charge/discharge the battery completely from completely discharged/charged state respectively in one hour. For instance, C-rate for 3.2 Ah battery is 3.2 A. If the battery is said to be charged with 0.5C or 1.5C then it indicates the charging current to be 1.6 A or 5.25 A respectively.

### B. Cycle Life

The battery is termed to be dead if its capacity drops to 80 percent of its initial value. The total number of charging and discharging cycles the battery can go through before its end of life is termed as Cycle Life of battery. Cycle life specified in the data sheet pertains to the specific testing conditions mentioned.

### C. Dual Polarization (DP) Cell Model

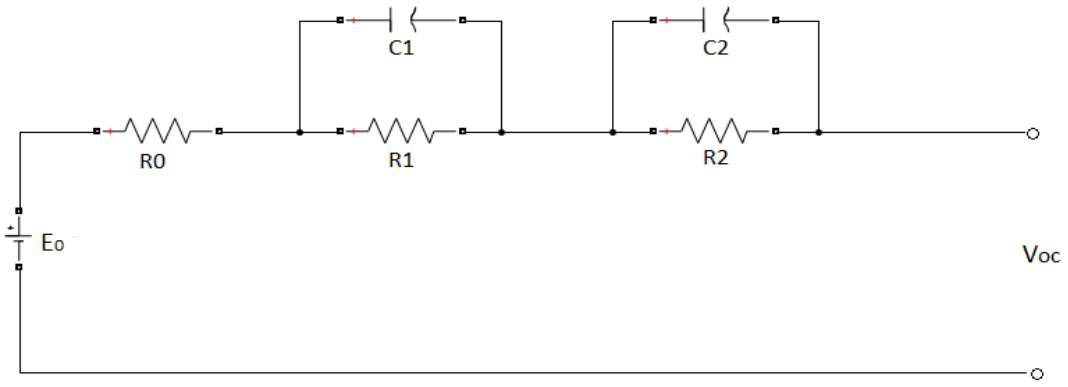


Figure 2. Dual polarization equivalent model of Li-ion cell.

According to the various experiments conducted on Li-ion cells, two types of polarization effects can be observed. This DP model as in Fig. 2 takes into consideration the effect of electrochemical polarization and concentration polarization separately which is exhibited by the two capacitances in the model. Thus the accuracy of this model is high.

$R_0$ is the ohmic resistance of the cell which includes the internal resistance and surface layer contact resistance of the cell. $R_1$, $R_2$, $C_1$ and $C_2$ replicate the dynamic operation of the cell. $V_{oc}$ is the open circuit voltage of the battery. $R_1$ is the electrolyte surface resistance and it characterizes electrochemical potential while $R_2$ is ion mobility resistance that characterizes concentration polarization. The capacitances $C_1$ and $C_2$ are used to depict the transient operation of the cell during charging and discharging process and to describe the electrochemical and concentration polarization effects respectively. $V_1$ and $V_2$ are the voltage drops across the resistances $R_1$ and $R_2$ respectively.

Based on the model in Fig.2, the following equations can be derived:

$$i_{bat} = \frac{V_i}{R_i} + C_i * \frac{dV_i}{dt}, \quad (i = 1, 2) \ldots\ldots (1)$$

$$V_{oc} = E_0 - V_1 - V_2 - (I_L * R_0) \ldots\ldots (2)$$

D. Open Circuit Voltage and SoC

The Open Circuit Voltage $V_{oc}$ of the cell is the function of cell SoC. The $V_{oc}$ of the cell represents SoC of the cell. There is non-linear relation between $V_{oc}$ and SoC of the cell which can be established by measuring $V_{oc}$ at different SoC states. SoC represents the available capacity of the battery and is generally calculated in percentage of available

capacity. Thus, SoC varies from 0% to 100%. In this paper coulomb counting method has been used to calculate the SoC of the cell. The law states,

$$SOC = SOC_{initial} - \eta \int_0^t i(t)dt \ldots\ldots (3)$$

Where, $SoC_{initial}$ is the initial condition of the battery. $\eta$ is the coulombic efficiency of the cell given by $\eta = \frac{1}{3600C}$ where C is the cell capacity and *i(t)* is the terminal current of cell.

The relation between $V_{OC}$ and SOC is non-linear and is determined by studying the graph provided in the data sheet. The relation between $V_{oc}$ and SoC can be obtained using the test procedure discussed in [5] and SoC vs $V_{oc}$ curve can be established. The points on the curve can be used as reference to predict SoC at different $V_{oc}$ conditions.

E. Transient Response

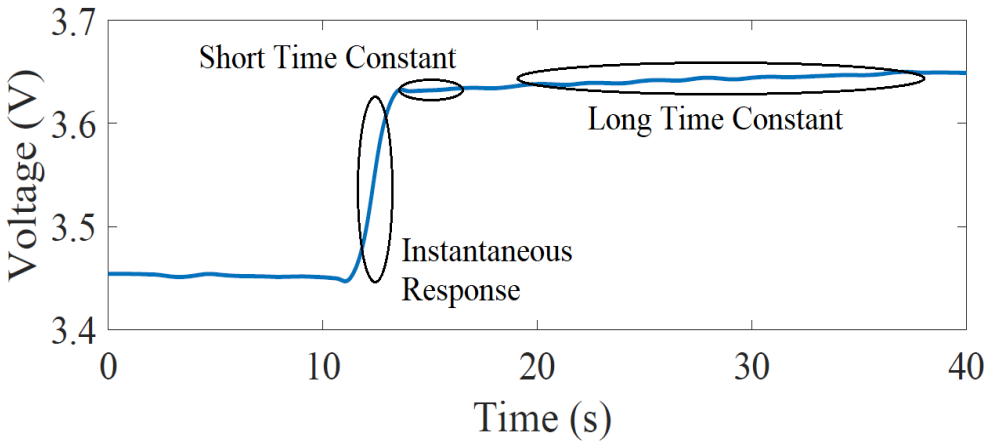


Figure 3. Transient response.

Figure 3 shows response of voltage to interruption in charging cycle. At t = 10sec the discharge process is interrupted, and the cell is open circuited. The voltage response can be divided into three parts. First being the steady state response namely longtime constant, second the transient response i.e. short time constant and the instantaneous step change. The $R_0$ is responsible for a step change in voltage also known as ohmic resistance of the cell. While $R_1C_1$ and $R_2C_2$ are polarization resistances reflected by the transient response of the cell. The Ro is responsible for the instantaneous voltage changes while $R_1C_1$ are responsible for short time constant and $R_2C_2$ are responsible for long time constant. All the circuit parameters in the model are multivariable functions of SoC. The procedure to calculate these parameters have will be discussed in following sections.

F. State of Health of Battery

State of Health (SoH) of battery represents the life of battery. A battery is dead when the maximum capacity of the cell decreases to 80% of its initial capacity under same test conditions. As per the experimental results there is no observable change in the polarization resistance due to ageing but the ohmic resistance changes distinguishably. Thus, the ohmic resistance can be considered as indicator of the age of the battery unit.

Generally, the maximum charging or discharging current of the cell is determined by

$$I_{max} = \frac{OCV - V_{min}}{R} \ldots \text{Charging} \ldots\ldots (4)$$

$$I_{max} = \frac{V_{max} - OCV}{R} \ldots \text{Discharging} \ldots\ldots (5)$$

Where, $I_{max}$ is the maximum current allowed to and from the cell, OCV is the Open Circuit Voltage of the cell. $V_{min}$ and $V_{max}$ is the voltage limits and R is the ohmic resistance of the cell.

State of Health (SoH), as the name suggests it represents condition of the cell in terms of its lifetime. The SoH of the cell depends on factors like, operating temperature of the cell and depth of discharge. During the testing regime, the temperature of cells was maintained constant at of 25ºC. Also, the depth of discharge was kept constant for each discharge cycle. Thus the aging effect due to these factors can be neglected in this case. According to [6], end of life can be defined when the resistance increases to the 160% of its initial resistance under same test conditions. The definition of SoH is:

$$SOH = \frac{R_{EOL} - R}{R_{EOL} - R_{new}} * 100\ \% \ldots\ldots (6)$$

Where, R is the current ohmic resistance of the cell, $R_{EOL}$ is the ohmic resistance when battery ohmic resistance reaches 160% of initial ohmic resistance and $R_{new}$ is the ohmic resistance of new battery unit. SoH is generally expressed in terms of percentage. When SoH is 100% it indicates battery is new while 0% SoH indicates the battery is dead i.e. at 80% of its initial capacity.

## IV. DERIVING $V_{OC}$ vs SoC RELATION

The equation used for calculating SoC is given in Eq.3. To calculate SoC during the battery operation we need to know the initial SoC of the cell. The $V_{oc}$ of the cell can be measured directly and knowing the $V_{oc}$ to predict the SoC of the cell. The relation between $V_{oc}$ and SoC can be obtained using following test procedure as used in [5].

Step 1: First the battery is completely charged. The battery is fully charged when the charging current is reduced to charge termination current which is specified in data sheet. This will be discussed in detail in later sections.

Step 2: After pausing for 1hr, the battery is then completely discharged and again completely charged after pause of 1hr. This makes sure the proper battery test conditions. The SoC of a cell is usually unknown and cycling it once with a defined waiting time before starting the actual test helps battery attain comparable test conditions.

Step 3: Then the battery is again charged and discharged with 1hr wait between two cycles. During charging and discharging, the process is paused after every 10% SoC change for short period of time to observe the dynamic behaviour of the cell/battery. A pause of 1hr is always applied between charging and discharging process to approach equilibrium and cool down.

Step 4: While discharging the voltage rises during the pauses. All voltages reached during the pauses at different SOC during discharging and charging are connected using a dotted line. The drop/rise in the voltage are not identical which suggest that the cool down time

is not enough to reach equilibrium state of the battery. The average curve of the dotted curves during charging and discharging is approximate OCV line.

In this manner SoC vs OCV curve can be established. The points on the curve can be used as reference to predict SoC at different $V_{oc}$ conditions during the battery operation. This type of testing is quite accurate and gives acceptable results for SoC range of 20% to 100% according to [5].

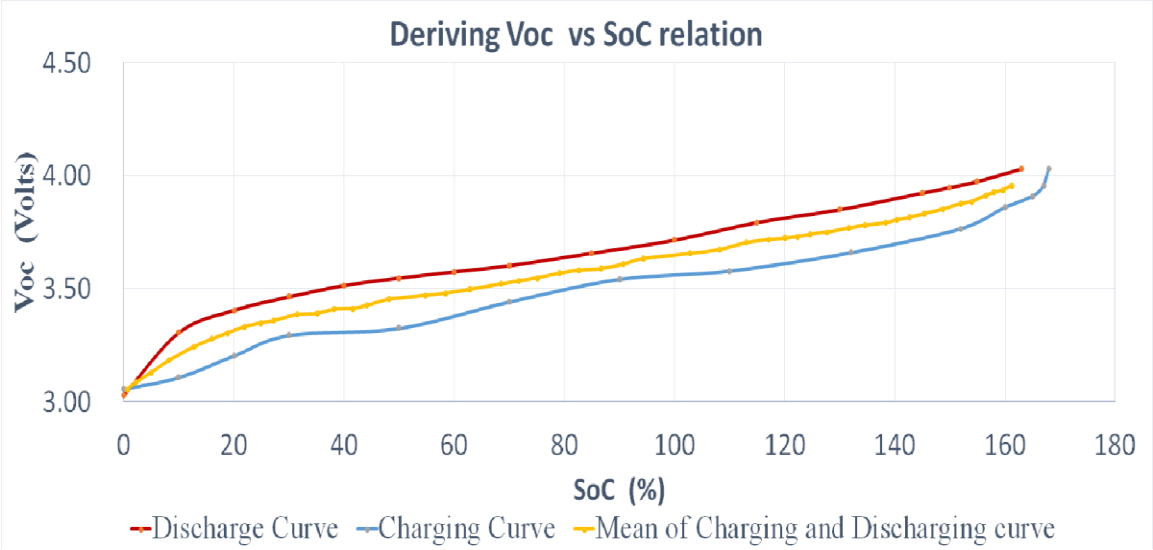


Figure 4. Voc vs SoC.

## V. PARAMETER EXTRACTION

To extract the parameters, we need to consider a pause during charging and discharging. Assuming during discharging process and the load is turned off at $t_0$, the instantaneous rise in voltage is due to the ohmic resistance $R_0$. By measuring the step change in voltage V and measuring the load current we can calculate $R_0$ using following equations:

$$\Delta V_{01} = |V_1 - V_0| \ldots\ldots (7)$$

$$R_0 = \frac{\Delta V_{01}}{|I|} \ldots\ldots (8)$$

Similarly, long time constant resistance $R_2$ can be calculated by:

$$\Delta V_{23} = |V_3 - V_2| \ldots\ldots (9)$$

$$R_2 = \frac{\Delta V_{23}}{|I|} \ldots\ldots (10)$$

While the short time constant resistance $R_1$ can be calculated by measuring the change in voltage during 5 seconds after instantaneous step change. Let the change in voltage be denoted as $\Delta V_{short}$. Then $R_1$ is given as:

$$\Delta V_{short} = |V_2 - V_1| \ldots\ldots (11)$$

$$R_1 = \frac{\Delta V_{short}}{|I|} \ldots\ldots (12)$$

The respective capacitances $C_1$ and $C_2$ can be calculated using the relation:

$$\tau = RC \ldots\ldots (13)$$

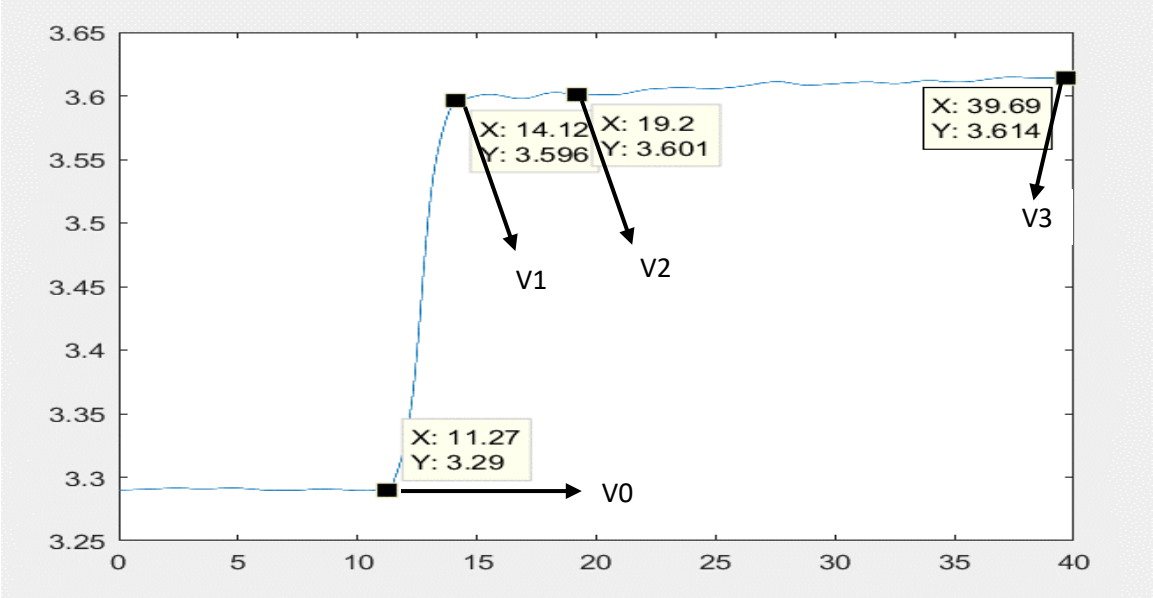


Figure 5. Dynamic response of battery.

The parameters obtained are then plotted for different SoC levels. The battery parameters are a function of SoC, temperature and cycle life. But a cooling fan is used to maintain the battery temperature constant and the cycles conducted in test are far too less compared to total life cycles. Also, study in [5] suggests these is no distinct change in parameter values with ageing effect for Li-ion batteries. Hence the effect of temperature and ageing have been neglected during parameter extraction. Thus, $R_0$, $R_1$, $R_2$, $C_1$, $C_2$ are all functions of battery SoC. Using this assumption and graphical plots generalized equations are computed to calculate the parameters at any given SoC conditions. The equations are as follows:

$$SoC = (0.2599*z^7) + (-0.0587*z^5) + (0.3226*z^4) + (3.553*z^3) + (1.421*z^2) + (31.61*z) + 49.66 \ldots\ldots (14)$$

Where

$$z = \frac{V_{oc} - 3.572}{0.249}$$

$$R_0 = -3E^{-07}(SoC)^3 + 7E^{-05}(SoC)^2 - 0.0053(SoC) + 0.244 \ldots\ldots (15)$$

$$R_1 = -5E^{-09}(SoC)^3 + 2E^{-06}(SoC)^2 - 0.0001(SoC) + 0.0128 \ldots\ldots (16)$$

$$R_2 = 3E^{-08}(SoC)^3 - 6E^{-06}(SoC)^2 + 0.0003(SoC) - 0.0023 \ldots\ldots (17)$$

Fig. 6 shows the plot for measured resistance values for a brand-new cell against the cell SoC.

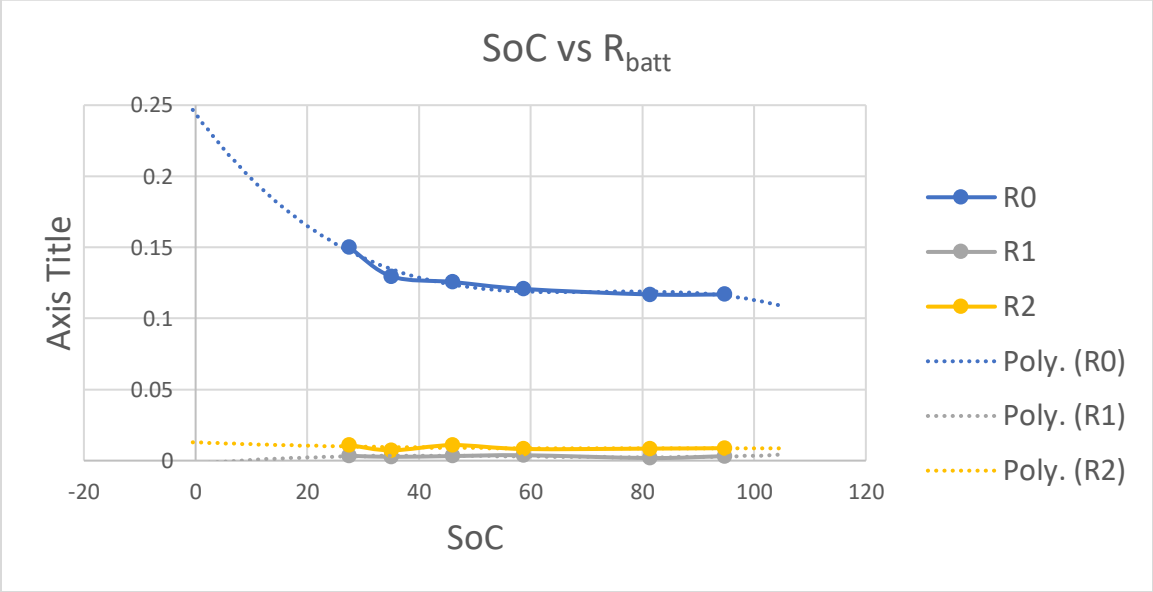


Figure 6. SoC vs Battery resistances.

## VI. MODEL VALIDATION.

The equations obtained above are then used in PLECS environment to simulate the DP model of the cell. The obtained simulation results are then compared with test results of the cell. The simulation model is an important tool which simplifies study of battery applications. For fast and accurate results, it is necessary to develop model which can replicate battery performance accurately.

Figure 7 shows the PLECS simulation model. This model uses the duel polarization model and incorporates few of the BMS features like voltage regulation with temperature change, safety switchover to prevent overcharging or over discharging of the battery.

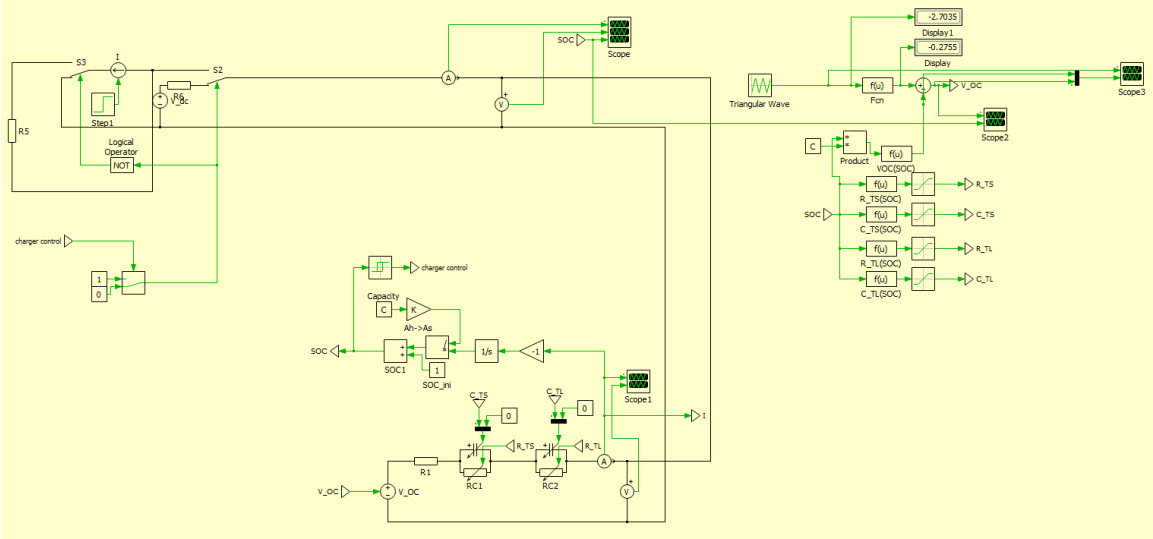


Figure 7. PLECS simulation model.

In this model the ohmic resistance is taken to be 0.1 Ω which is the average value obtained after testing multiple cells. It is considered to be a constant value as it remains same over nominal operating range of 40% to 90% SoC. The same can be seen form

Fig.6. The values for polarization resistances/capacitances and $V_{oc}$ are calculated from SoC value are as per equations (13) through (16).

Figure 8 shows the charging and discharging characteristics of the Li-ion cell. This model replicates the performance specifically of NCR 18650 cells. Fig. 9 shows the effect of change in operating temperature on charging and discharging characteristics of the cell. The relation between temperature and open circuit voltage has been discussed in [11].

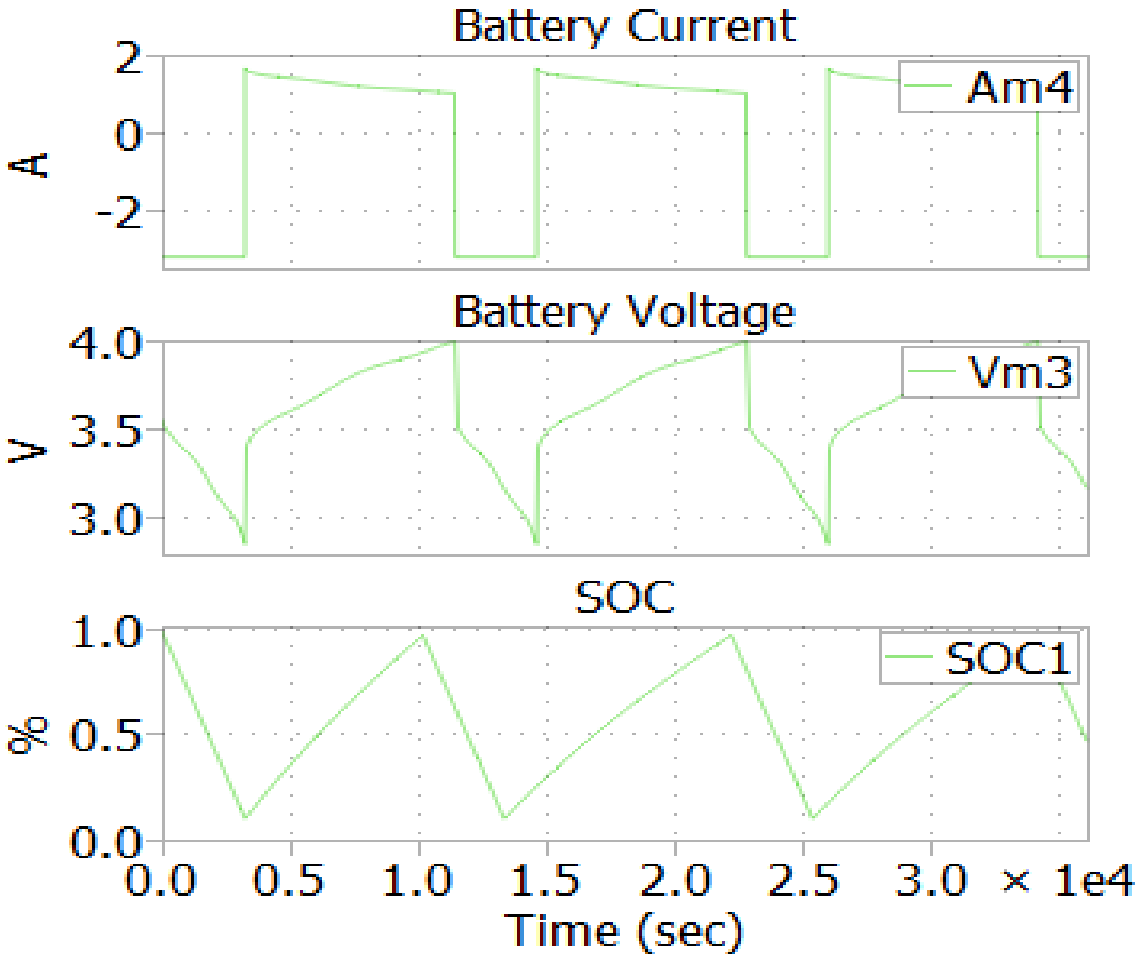


Figure 8. Charging and Discharging Characteristics.

Fig.8 shows the battery current, battery terminal voltage and corresponding cell SoC.

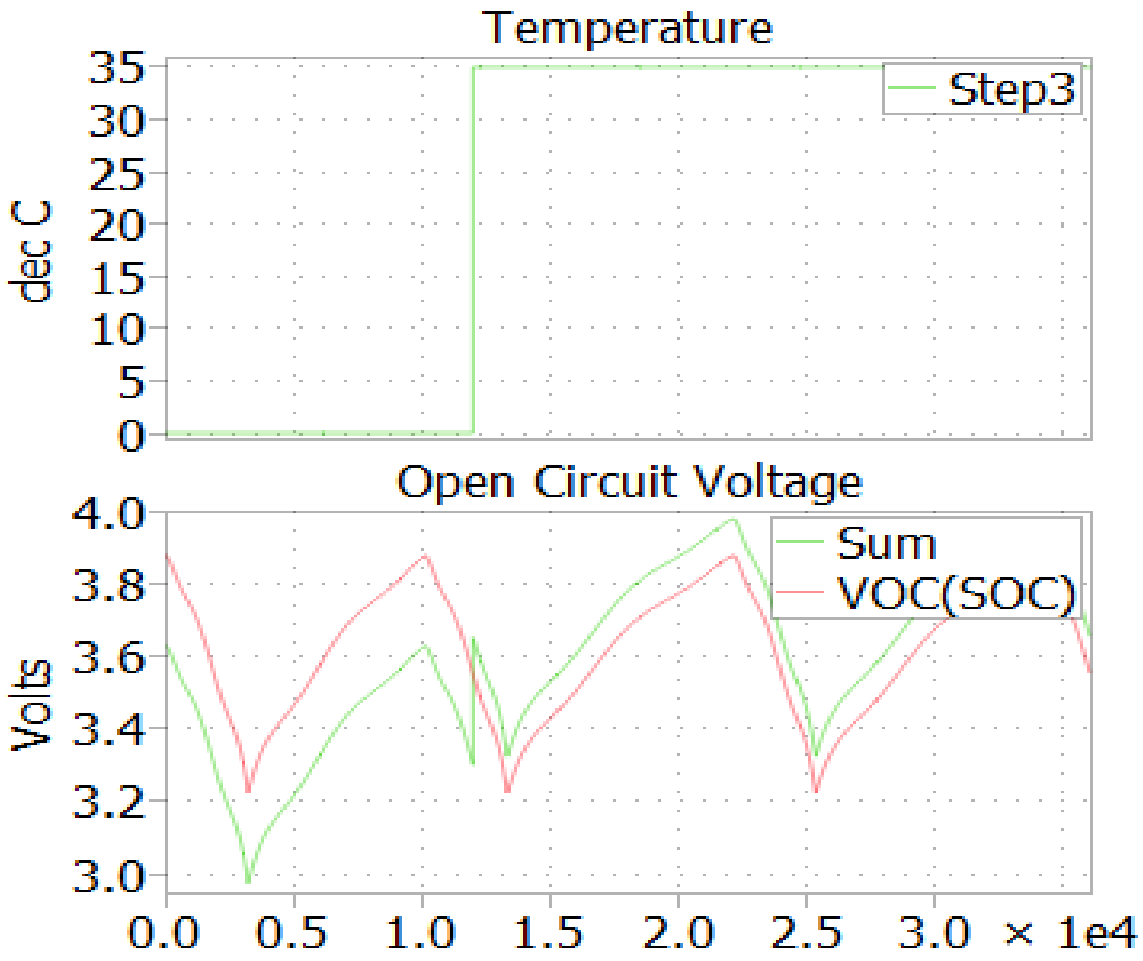


Figure 9. Effect of temperature on Cell Voltage.

In fig. 9. initially the cell temperature is $0^0$C while after 12,000 s it is change to $35^0$C. The effect of change in temperature can be seen in the plot labeled Sum. While the plot labeled VOC(SOC) shows cell operation at room temperature of $23^0$C. Generally, the cell rated voltage is specified at room temperature. It can be clearly observed that cell open circuit voltage drops below rated value while it is higher than rated value for lower and higher operating temperatures respectively. Hence careful design of cell protection circuitry and cooling/heating mechanisms need to be done as per the conditions pertaining to the application.

# VII. BATTERY MANAGEMENT SYSTEM (BMS)

The priority task of BMS is to make sure that the battery is used efficiently while supplying the load and to prevent damage to the battery. This can be achieved by control and monitoring of charging and discharging process of the battery. Thus, BMS implements control and monitoring of battery charging and discharging regime.

There are main algorithms to check and control the links in the energy chain. These have been listed as follows:

i. Charging Algorithm:

These tracks and controls the charging by interrupting it when the battery is full. Overcharging leads to increase in battery temperature. This leads to damage of the battery decreasing the capacity and useful cycles. Proper charging algorithms are necessary for efficient battery usage.

ii. Discharge Algorithm:

This controls the magnitude of the discharge current. It makes sure that that the discharge current does not exceed the rated/set current limit of the battery discharge current. Also, it isolates the battery from the load if the operating voltage falls below safe limits thus preventing permanent damage to the cell due to over discharge.

iii. Algorithms to determine SOC:

This algorithm is used as a feedback to the charging algorithm to end charge and discharge cycles, as aforementioned discussions.

iv. Algorithm to control DC-DC converter(Charger):

This is used to power the load with minimum required voltage.

Objectives of Battery Management System:

1. Battery Management -Optimum use the battery
2. Power Management- Minimum power dissipation and proper power distribution.
3. Energy management -Efficient energy conversion
4. Keep track of SOC-SOC is used to control charging and discharging.

Thus, BMS integrates two functions of monitoring and control. The monitoring unit collects the data specific to the battery such as the charging or discharging currents, SoC, number of cycles, and depth of discharge. While the control unit is the one which implements intelligence to the system by acting on the charging and discharging processes based on the data collected by the monitoring unit. A BMS system can be made very sophisticated for optimum use of the battery but is subject to various considerations:

a. Cost of the Product: The cost associated with the BMS should not overwhelm the cost of the product. For instance, the BMS implemented in a cell phone should not be very advanced such that it contributes to majority of production cost.
b. Product Requirement: The BMS should be designed as per the product requirement. Certain applications use batteries in sensitive environment and call for high level BMS system. For instance, in Electric Vehicles harbor large battery packs, inadequate BMS can lead to overheating of batteries which in turn cause the batteries to blast leading to fatal accidents. Hence sophisticated BMS needs to be implemented in such applications.

c. Types of Batteries: Certain batteries are more sensitive than others and require better monitoring.

A generalized battery management system can be represented using following block diagram:

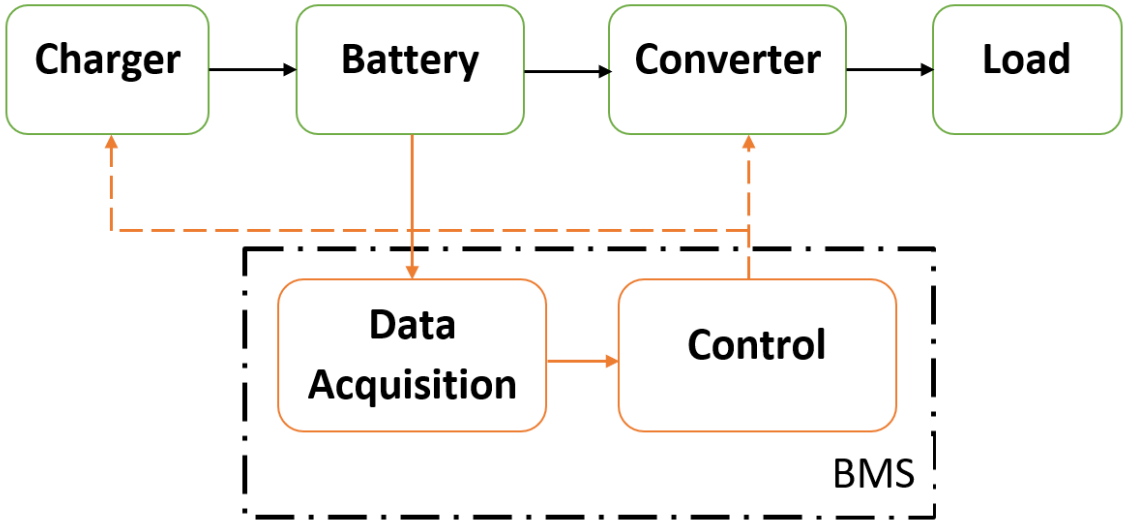


Figure 10. BMS block diagram.

The Orange channels show the communication channel while the black arrows denote electrical connections. The data acquisition unit and the control unit together form the BMS. The data acquisition unit is the monitoring unit that records real time data from the battery like the charging and discharging current, SoC of the battery, etc. depending on the sophistication of the BMS and the parameters required to be monitored. The data is then given to the control which uses it as reference data to generate control signals for the charger and converter units. The converter, which is a DC-AC or DC-DC unit depending on the load, is used to interface the load with the battery thus controlling the discharge rate while the charging unit (AC-DC or DC-DC) is required to charge the battery. The

charging unit can also directly power the load in most applications like portable electronics. The main BMS components are as follows:

A. Charger

Charger can also be referred to as the power module. The power module is generally a AC-DC converter which can be plugged into the mains supply. When the battery is running low, the charger can be used to power the device directly while simultaneously charging the battery. And supply the load bypassing the battery when fully charged to preserve the charge for later use when mains supply is not available.

The BMS must control two parameters for the charger. First the energy conversion process and the charging parameters of the battery. The charging current and voltage of the battery is continuously measured and fed back to the controller of the BMS. Which in turn generates the control signal to control the output of the charger. For instance, in simple converter it generates the duty cycle signal to control the switching of the power devices (MOSFET or IGBT) to adjust the output.

B. The Battery

Main function of the battery is to store energy. The BMS should be designed specifically for a certain battery type.

a) Electronic Safety Switch for Li-ion batteries.

Li-ion batteries are very sensitive and require a safety switch to be integrated with the battery. Operating Li-ion cells outside the safe operating region can be hazardous. For

li-ion batteries the safe operating region is defined by the operating voltage, charging/discharging current and the operating temperature. Operating the cell outside safe region high voltages can cause the cell to cause fire or explosion and at low voltages it might cause irreversible losses to the overall capacity.

Maintaining the battery at high voltage increases the battery capacity of the battery but reduces the cycle life considerably. So, the allowable maximum charging voltage is a trade of between cycle life and capacity. Higher the operating current more is the operating temperature of the battery. Depending upon the operating conditions and application of the cell, the limit for the maximum current should be decided. Both the max voltage and max current limits should be within the safe area of operation. Once the limits are set, the electronic safety switch can be controlled using a controller.

The electronic safety switch is generally a MOSFET in series with the battery. The controller senses the voltage of the battery and the current and generates isolation signal whenever any set limit is exceeded.

b) Charge Balancing

A single Li-ion cell can produce voltage around 3.6V and provide around 6A of max current. This is too small for most of the applications i.e., electric vehicles. For this purpose, number of cells are connected in series and parallel to derive the required rating. Adding cells in series increase the voltage while adding cells in parallel increases the current rating of the battery.

Two identical cells used for same application show difference in their performance. This is due to the variations occurred during manufacturing, difference in impedances, unequal heat distribution to the packaging style, etc. These variations become even more severe with ageing effect.

Due to this difference in SoC levels is observed across different cells during charging and discharging processes. There are many supervisory ICs available commercially. These ICs supervise individual cell voltages and interrupt charge or discharge currents when one of the voltage set limit is exceeded. A charge balancing circuit equally distributes the charge applied to or drawn from the battery between the individual cells by transferring charge from highest SoC cell to lowest SoC cell.

c) Smart Battery

Smart battery is a battery with a microchip installed on it. This chip implements the functions mentioned above with certain other functions like communication with the host and calculate and predict Real-time battery information. Smart battery comes with features such as, self-monitoring, charge control, fault identification, protection and communication with host to store data. Once you have the first two features in the battery it is relatively inexpensive to add the additional features.

C. DC-DC Converter

The DC-DC converter is used to interface the battery to the load. The battery rating may not be the same as the load demands. The DC-DC converter is in charge of

providing appropriate voltage and current as per the load demands. This ensures efficient use of the battery and monitors the discharge current.

The converter is controlled by a microcontroller. The controller senses the battery parameters to be controlled and load requirements and generates appropriate control signals to adjust the converter output.

## VIII. LI-ION CELL OPERATING CHARACTERISTICS

There are 2 charging modes for Li -ion batteries.

1. Constant Current (CC mode)
2. Followed by constant voltage (CV mode)

The max voltage is determined by 2 factors. Firstly, the max battery capacity and secondly its cycle life. Battery's life ends when capacity drops below 80% of the initial value.

Max capacity is proportional to Max charging voltage. Life of the battery is inversely proportional to charging voltage. 10mV increase in battery voltage yields 12% increase in capacity but decrease in life cycles by 200.

The same is shown in fig.11 as illustrated in [9]:

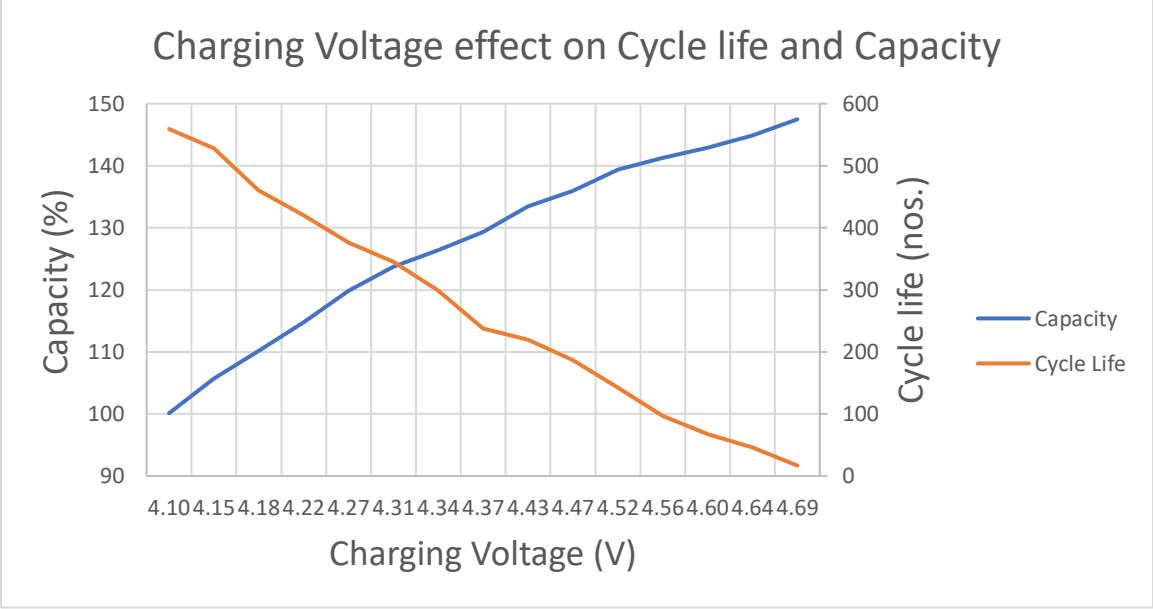


Figure 11. Max battery capacity and cycle life of battery voltage

The following figure shows V and I characteristics during the application of a CC/CV charging regime to Li-ion battery.

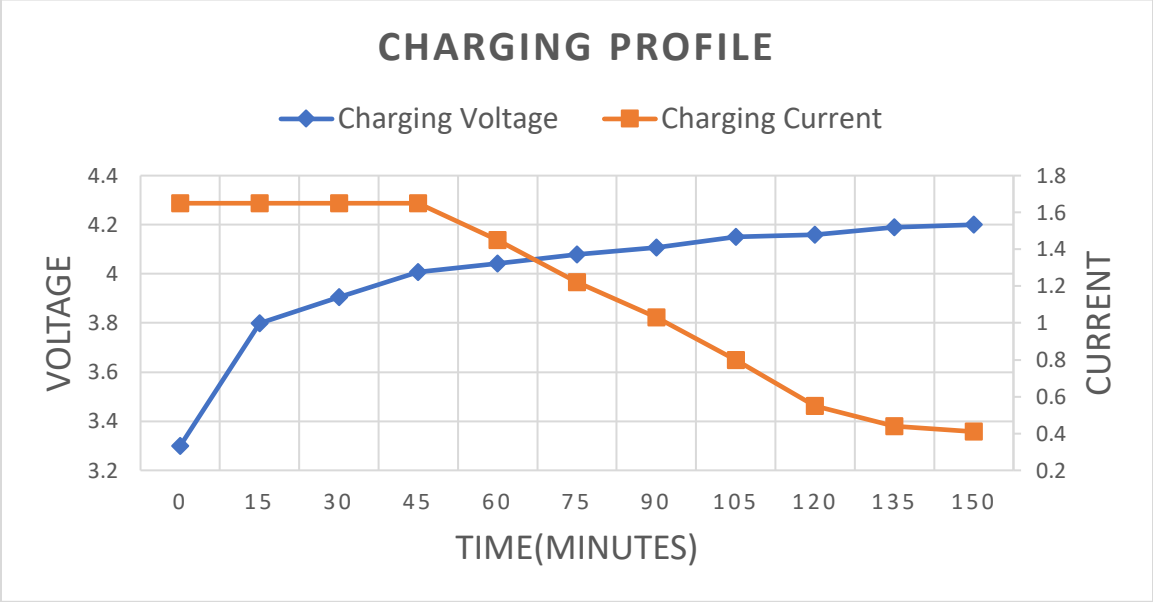


Figure 12. Charging V/I characteristics

Both $I_{cc}$ and $V_{max}$ values are specified by the battery manufacturer. Charge rate is generally around 0.7C to 1C which is related to the allowed current density. Value of $V_{max}$ is either 4.1V±1% or 4.2V±1%.

(A high degree of accuracy is taken care when specifying the value of $V_{max}$. This is because battery manufacturers want to guarantee a certain and a certain cycle life). $I_{min}$ is chosen to be 0.05C to 0.1C.

A. Charge Termination Mechanism

$I_{min}$ and $t_{max}$ both can be used as charge termination point. But there is a difference between using $I_{min}$ and $t_{max}$ as charge termination point. The advantage of using $I_{min}$ is

that the battery is then charged to full battery capacity. The time for which the battery is in CV mode is reduced which is advantageous to the battery's cycle life. The difference between the externally applied charging voltage $V_{max}$ and battery's equilibrium potential E determines the current that flows into the battery in CV mode. The difference is equal to η (over potential) including ohmic potential drop.

The battery's SoC, impedance, current and temperature determines the total overpotential of the battery. When charging is stopped at current $I_{min}$, this occurs at same SoC under the condition of constant temperature and internal impedance. Using equation $E=V_{max}-\eta$, we can find out the value of SoC, where SoC is the only unknown quantity.

The current value will not necessarily stop at the same value when the charging is stopped at $t_{max}$. For example, when a half-full battery is charged with as charge time $t_{max}$ the current at the end of charging will be different from the situation where an empty battery has been put on charge for the same charge time of $t_{max}$. Therefore, the starting SoC and the ending SoC will not be the same. This poses a problem for Battery Management System algorithm.

B. Protection

A Li-ion battery needs to be charged within a certain battery voltage and temperature range. Charging stops when the battery voltage or temperature is outside the specified range. Before charging the battery, the charger checks for the fault conditions, such as short circuit or open circuit. To be safe, an electronic switch is always connected in series with a Li-ion battery which will interrupt the current flow when the battery is out

of the specified range. The safety voltage and temperature are wider than the ranges for safety. Hence, the safety switch will be able to interrupt the charge current when the charger safety fails. For extra safety, device such as Positive-Temperature Coefficient resistor (PTC) is also connected to prevent failure.

C. Charging Voltage

A higher value of $V_{max}$ leads to higher capacity, but at the same time the cycle life decreases drastically. One of the reason for the loss of cycle life is the decomposition of the electrolyte at a higher value of voltage. A high value of voltage is present at the positive electrode when the battery is charged in CV mode. During the decomposition reaction, the $Li^+$ ions react irreversibly with the compounds of the electrolyte to form decomposition products. The longer the battery remains at the relatively high CV voltage, the more electrolyte will be decomposed, using up valuable active material, thereby lowering the capacity. So besides high value of $V_{max}$, the application of $V_{max}$ for long periods of time should be avoided.

D. Charging Current

The battery can be charged quickly to the set max charging voltage $V_{max}$ if higher charging current is utilized. But it was observed that there is no significant decrease in full charge time even if higher charge current is used. The reason being, under constant voltage charging regime, the current decays exponentially hence the time required to completely charge the battery does not reduce significantly.

But using high charging current causes loss in capacity of the cell. A possible cause of capacity loss could be Li metal deposition as the negative electrode potential drops below 0V. Higher the current lower is the potential drop below 0V. This causes irreversible Li metal deposition on the negative electrode.

# IX. MULTILEVEL MODULAR CONVERTER BASED BESS

MMC is gaining popularity in medium to high voltage applications due to advantages like low harmonic content on AC side, scalability and high reliability due to modular structure. Due to these features, it reduces the size of filters required on grid side, due to scalability there is no need of step up transformer and due to modular structure, it reduces the down time.

Renewable energy sources are very uncertain and not constant. To overcome these power fluctuations, energy storage systems are required in renewable energy systems to maintain grid stability. Li-ion batteries due to their high energy density and stability are replacing the traditionally used lead acid batteries in Battery Energy Storage systems which are being used widely renewable energy generation facilities.

Integration of Battery Energy Storage into the MMC has been discussed in [2]. MMC can use balancing of battery SoC in each submodule thus preventing overcharge or discharge which may damage the batteries. Moreover, it can utilize the circulating currents to improve the internal regulation capability and output power quality.

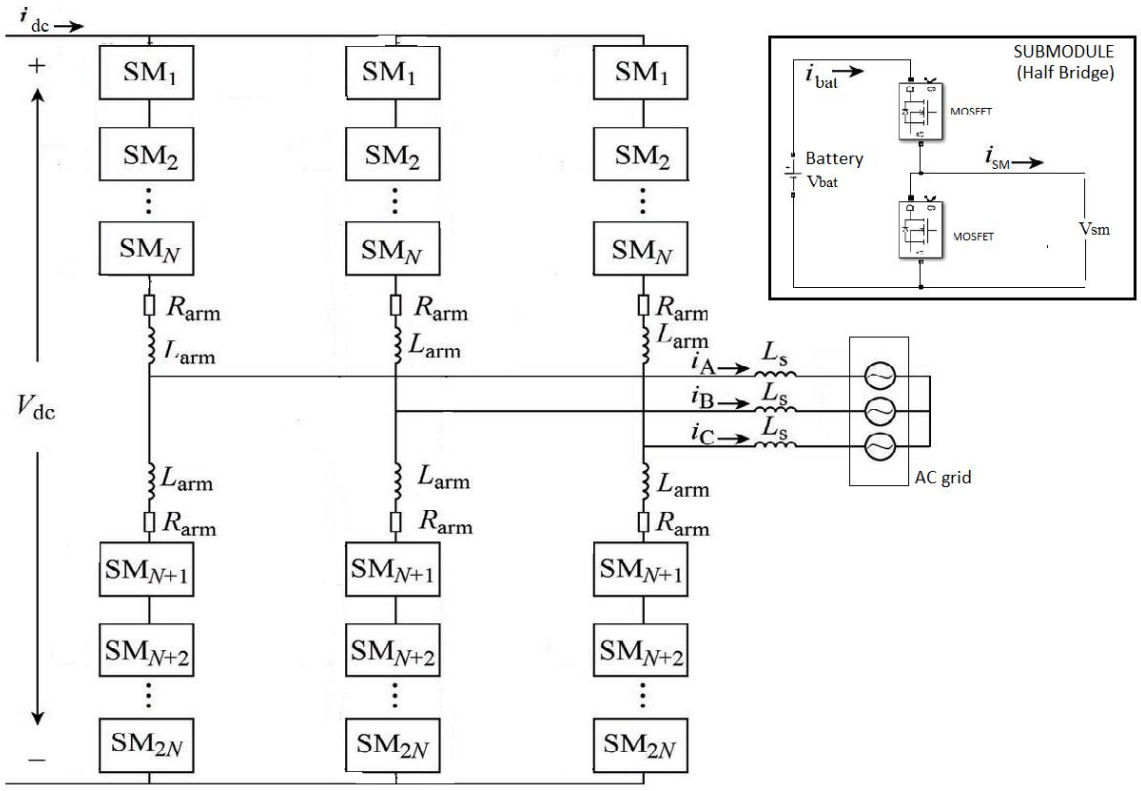


Figure 13. MMC based BESS.

Figure 13 shows BESS integrated into MMC. But in case of MMC, the output voltage of each submodule is given as:

$$V_{sm} = \frac{V_{bat}}{2} - \frac{V_{bat}}{2} * d \ \ldots\ldots (18)$$

Where d = m* sin(ωt)

m= modulation index

The arm current of MMC represented by $i_{arm}$ is given by (19), which equals to the SM current:

$$i_{arm} = i_{sm} = \left(\frac{i_{dc}}{3}\right) + \left(\frac{I_m}{2}\right) * sin(\omega t) \ \ldots\ldots (19)$$

Where, $I_m$ denotes the magnitude of phase current.

$$P = V_{sm} * i_{sm} = \left(\frac{i_{dc}}{3}\right)\left(\frac{V_{bat}}{2}\right) - \left(\frac{i_{dc}}{3}\right)\left(\frac{V_{bat}}{2}\right) m\, sin(\omega t) + \left(\frac{I_m}{2}\right)\left(\frac{V_{bat}}{2}\right) * sin(\omega t)$$

$$- \left(\frac{I_m}{2}\right)\left(\frac{V_{bat}}{2}\right)\left(\frac{1 - \cos(2\omega t)}{2}\right) \quad \ldots\ldots (20)$$

$$i_{bat} = \left(\frac{i_{dc}}{6}\right) - \left(\frac{i_{dc}}{6}\right) m\, sin(\omega t) + \left(\frac{I_m}{4}\right) sin(\omega t) - \left(\frac{I_m}{8}\right) + \frac{I_m \cos(2\omega t)}{8} \ldots\ldots (21)$$

Maximum ripple is observed for $i_{dc}$=0

$$i_{bat} = \left(\frac{I_m}{4}\right) sin(\omega t) - \left(\frac{I_m}{8}\right) + \frac{I_m \cos(2\omega t)}{8} \ldots\ldots (22)$$

Thus, it can be seen that, there is power line frequency component and second harmonic component present on the DC side of each submodule. Figure 14 shows the frequency spectrum of the frequencies observed on DC side of each submodule from PLECS simulation of MMC using BESS and half bridge submodules. It can be seen that in a submodule, on DC side there is large amount of ripple. The fundamental component can be as high as 200 percent while the 2nd harmonic content is 100 percent of the DC component. In order to integrate BESS into the MMC, it is important to evaluate the effect of ripple content on the battery performance. Due to voltage imbalance between the phase arms circulating currents flow between the arms. Harmonics of circulating currents are even harmonics excluding tripleen harmonics. The 2$^{nd}$ harmonic is prominent compared to other harmonics. Thus, the submodule has to supply both the arm current

and circulating currents which leads to presence of large ripple content on the DC side of the submodule.

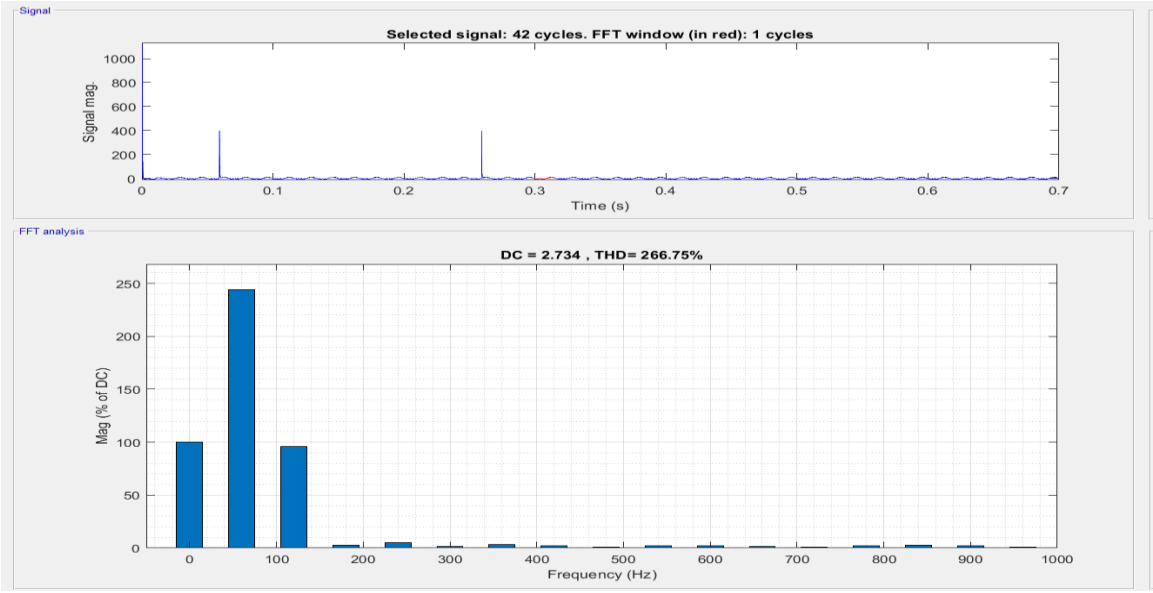


Figure 14. Frequency spectrum of DC side MMC current waveform.

# X. EXPERIMENTAL SETUP

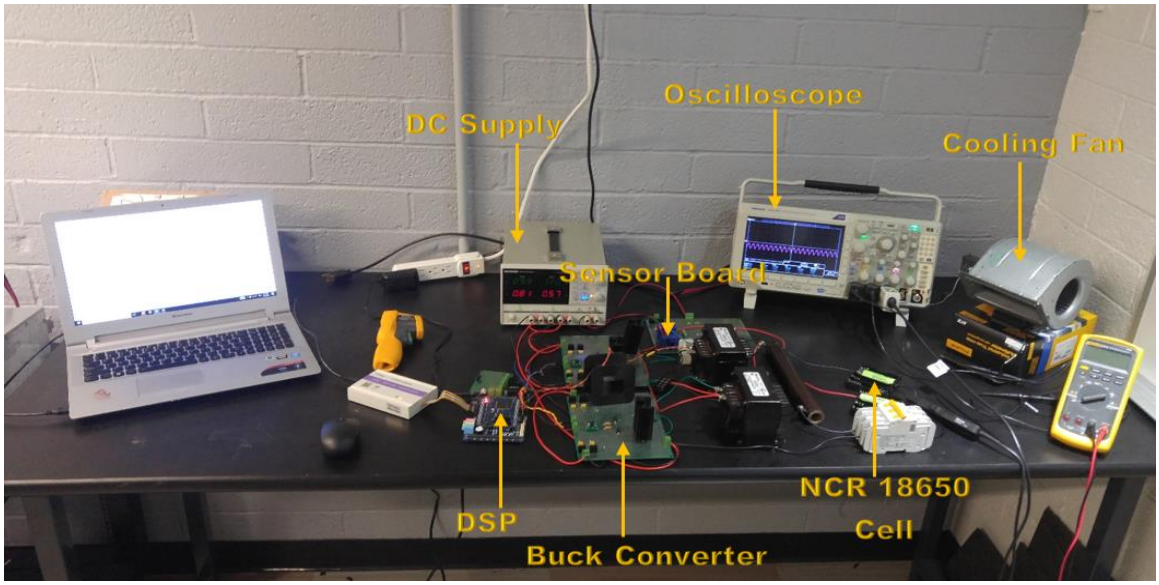


Figure 15. Experimental setup

## A. Converter

The converter used for the experiment purpose is effectively a buck converter topology. The control signal for the converter was generated using the Texas Instruments DSP F28335. The code for the DSP was written using the Code composer studio software and the DSP was interfaced to the computer using an emulator.

The control strategy implemented was that of SPWM. The converter utilized Infineon MOSFET (IPP075N15N3 G). This MOSFET is an n-channel power transistor rated at 100A and 150V.

For the experiment, the output current was controlled using PI and PR controllers of the DSP. The code used for this purpose has been illustrated in appendix B. The converter was effectively used to generate charging and discharging currents of 1.65A

DC and to add required ripple content to the DC current for study purpose. For charging stage, the DC supply by GW Instek was used to provide constant voltage source of 10V. While for discharge stage, the Li-ion cell under test was used as constant voltage source.

B. Current and Voltage Measurement.

For monitoring current and voltage at the output of the converter, current and voltage transducers by LEM were utilized. The current transducer was of LA 55-P and voltage transducer LV 25-P series.

LA 55-P is suitable for DC and AC current measurements and provides galvanic isolation between primary circuit (high power) and secondary electronic circuit. It is a closed loop current transducer which operates on principle of Hall Effect.

LV 25-P transducer is similar to LA 55-P in terms of operating principle. For voltage measurements, a current proportional to the measured voltage must pass through the measurement resistor. The measurement resistor is selected by the user and is installed in series with primary circuit of the transducer.

The circuit diagrams of all electronic circuits were developed using ALTIUM software. Figures 16 and 17 show the circuits used for the testing purpose.

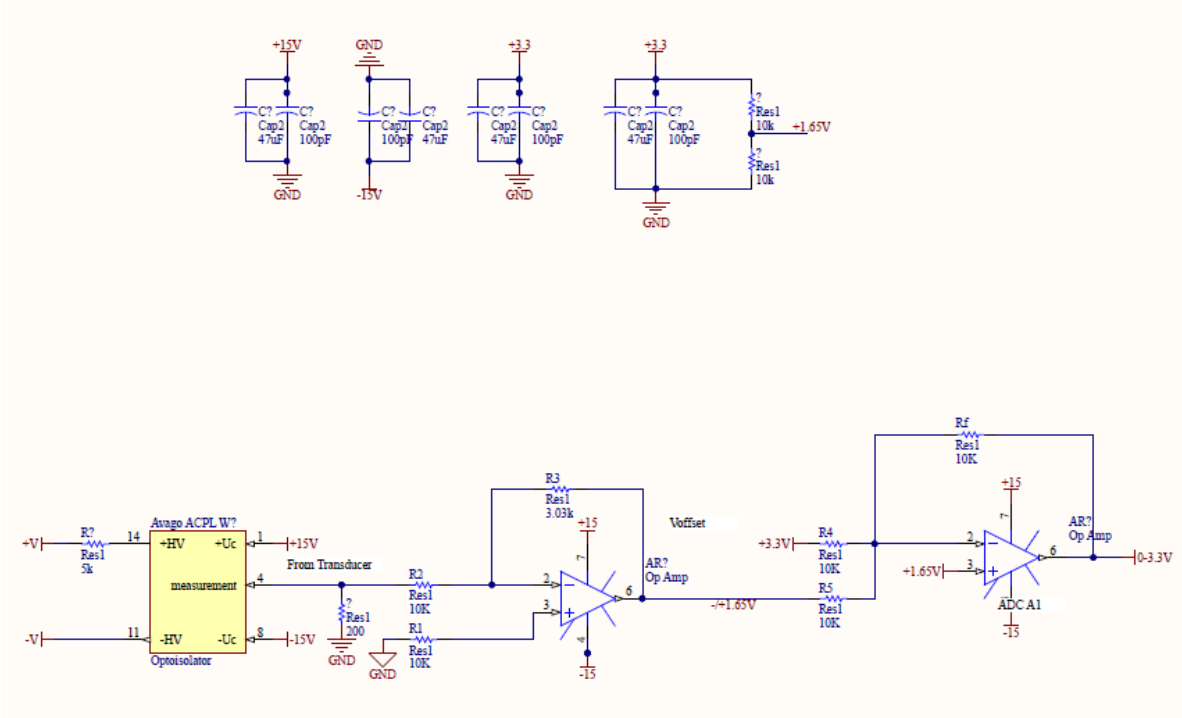


Figure 16. Voltage transducer schematic

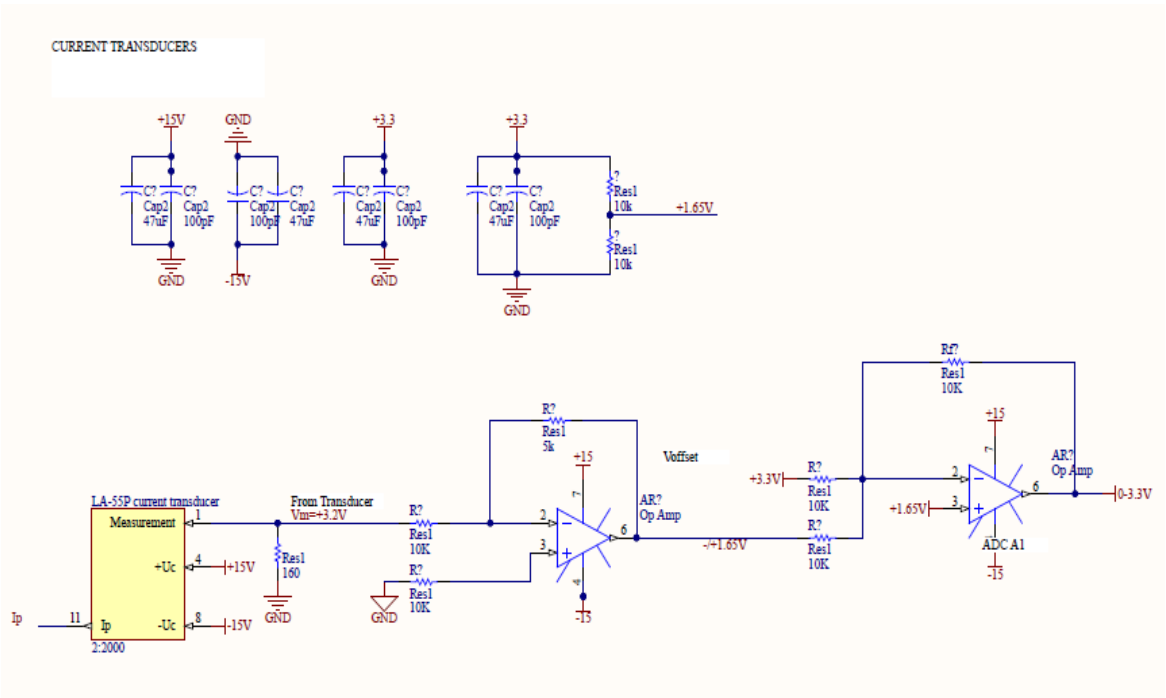


Figure 17. Current transducer schematic

Following the transducer unit, the output of the transducer is fed to an amplifier circuit and then to bipolar to unipolar converter. The converter converts the output of the transducer which is bipolar (both positive and negative values) to unipolar output suitable to feedback to ADC of the DSP. In this case the voltage transducer output is ±3.3 V which is converted to ±1.65V by the amplifier stage and then to 0-3.3V by the converter stage. The input range of the ADC of DSP is same 0-3.3V.

C. Gate Driver

The gate driver is an important circuit pertaining to the Buck converter. Gate driver by Avago ACPL-W345 was used to generate the gate signal. ACPL-W345 contains an AlGaAs LED, which is optically coupled to an IC with power output stage. This diver is suitable for generating gate signals for MOSFETs used in any type of converter systems. The gate driver can generate gate voltage of ±20V and max output current of 1A. The high O/P current and voltage make this driver suitable for direct driving MOSFETs at high frequency for high efficiency conversion. For this experimental purpose, the output voltage of the driver circuit was set to +15V and -5V DC. Figure 18 shows the diver circuit. A series resistor R3 is used to limit the gate current as per the MOSFET rating. Also, antiparallel Zener diodes are used to protect the MOSFET gate from over voltage conditions.

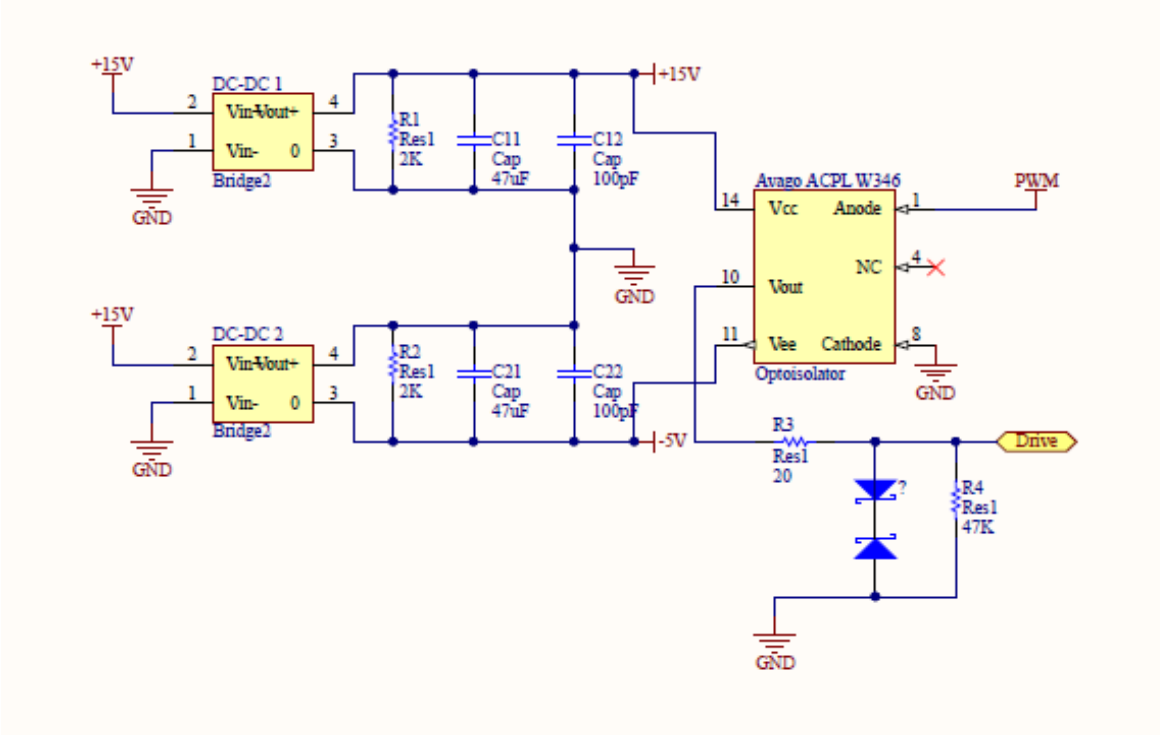


Figure 18. Gate driver circuit

D. Peripheral Equipment

All the waveforms for the purpose of study were monitored and recorded by using the Tektronics MDO3000 series Oscilloscope. A cooling fan was utilized to keep the operating temperature of the cell under test constant at room temperature.

## XI. TEST PROCEDURE

The current waveform obtained from the simulation results of MMC was recreated using the DSP controlled buck converter. Fig.19 shows the waveform obtained from the PLECS simulation, while Fig.20 shows the current waveform used during testing procedure. The nature of the waveforms is similar with respect to harmonic content. Using this waveform, a cell was charged and discharged multiple times and the resistance was calculated from transient response as discussed in earlier sections. The resistance was calculated before and after the test procedure and were compared. Different cells were tested in same fashion but with different magnitude of current ripple. The experimental results of all cells were then compared to determine the effect of ripple on lifetime of the battery.

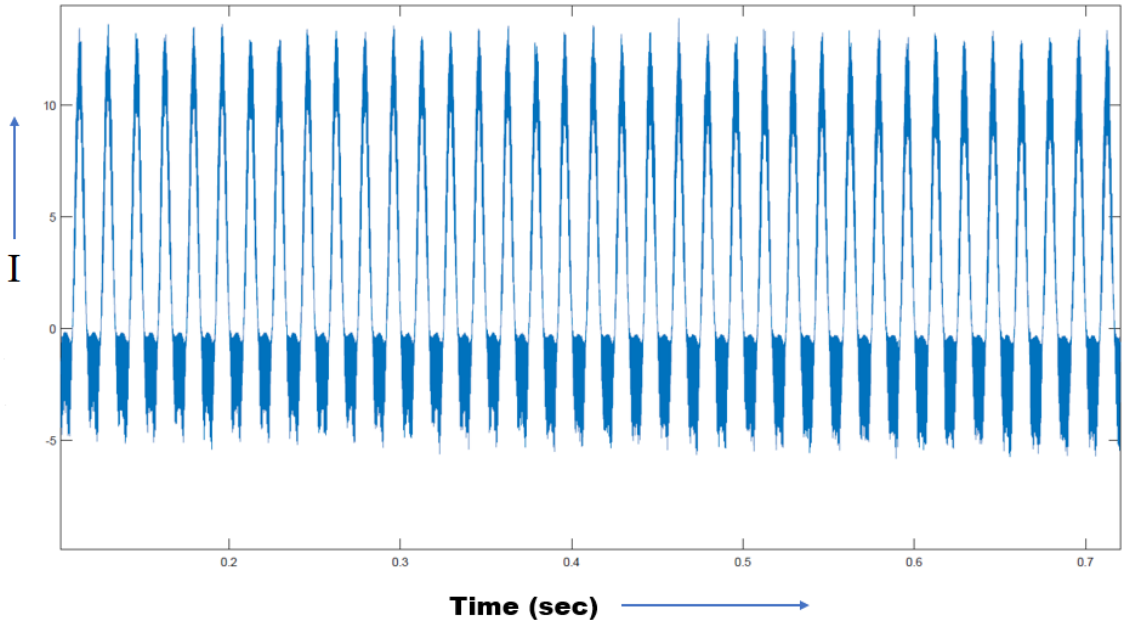


Figure 19. PLECS simulation MMC waveform

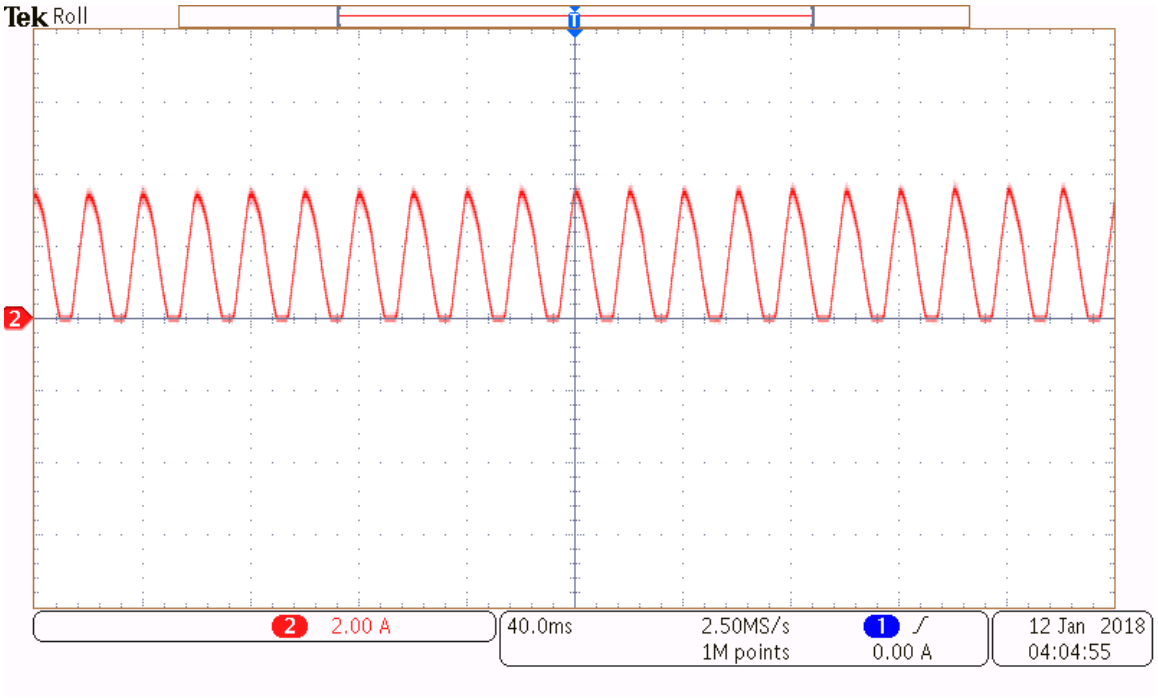


Figure 20. Test waveform

The nominal voltage of the battery is 3.6V which can be known from its data sheet. Generally, in BESS the voltage of batteries is balanced and maintained above the nominal value. The nominal voltage of this battery corresponds to 60% SoC and hence, SoC between 40% to 90% was identified as the operating range. The resistances corresponding to this operating region were compared.

The testing was conducted on various cells with ripple percentage varying as 0, 5, 10, 20 percent (60 Hz fundamental frequency ripple) and then tested using the waveform observed from MMC simulation. Cell with 5% ripple content showed an increase of 9% ion cell resistance. While cell tested with 10 percent ripple content showed average increase in resistance by 17 percent in the measured SoC range. Further, the cell tested

with 20 percent ripple content showed increase of 19 percent in cell resistance. While the cell tested with waveform similar to that observed on DC side of MMC submodule showed increase in cell resistance by 29 percent.

The degradation of cells in terms of SoH of the battery is illustrated in Fig.21. Which is calculated using Eq.6.

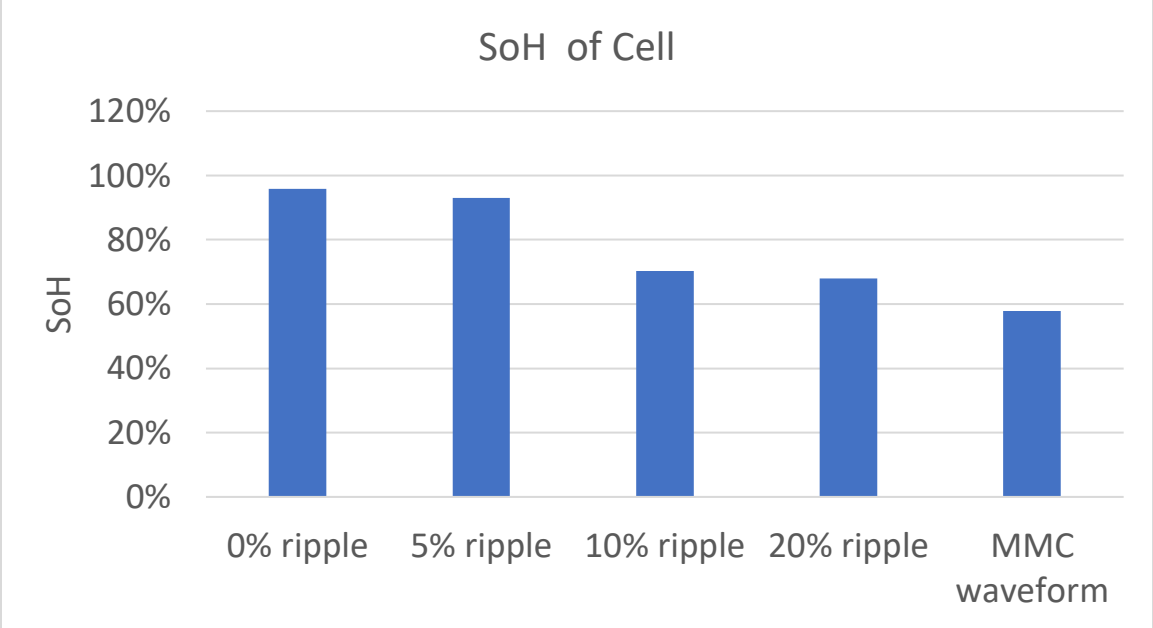


Figure 21. Current SoH of the cell

SoH represents the condition of the cell. 100% SoH corresponds to new cell with no loss in capacity. While 0% SoH corresponds to dead cell with capacity reduced to 80%. To confirm the test results, the cell tested with MMC waveform was tested for another 10 cycles with same waveform. After the test, capacity test was conducted on the cell. For capacity test, the cell was first charged completely to 100% SoC and then discharge using 1.4A discharge current. The cell was discharged completely in 1.9 hours. Thus, the capacity of the cell was 2.66 Ah against 3.2Ah rated capacity, i.e., the capacity

of cell was reduced to 81%. This verifies the test results. For 10 cycles increase in resistance was 29% thus it indicates slightly above 50% SoH. In another 10 cycles, the cell was reduced to almost 0% SoH.

Same test was conducted again on a brand-new cell which was cycled 20 times. After 20 cycles it showed 59% increase in cell resistance which indicates near 0% SoH (0% SoH corresponds to 60% increase in cell resistance).

# XII. PASSIVE FILTERING

As it can be seen that low frequency ripple has negative impact on life time of the battery, it is necessary to reduce the ripple content observed by the battery. One way to achieve the same is using capacitive filter on the DC side of the MMC submodule. As on DC side of the MMC, fundamental and second frequency harmonics are dominant, the filter needs to be designed accordingly. The impedance of the capacitive filter observed by the ripple needs to be lower than that of the battery itself. The impedance of the capacitive filter for particular frequency is given by:

$$Z = \frac{1}{2\pi f C} \ldots\ldots (23)$$

Where, f is the frequency and C is capacitance of the filter.

For negligible effect on life time of the battery, it is necessary to reduce the harmonic content in the system below 5%.

To analyze the same, a capacitive filter is simulated using MATLAB. Figure shows the simulation model used to observe effect of using a capacitor in parallel with the battery. Using a capacitor, it creates a low impedance path for ripple current while it is observed as open circuit by DC current. As a result, the ripple current flows through the capacitor and battery doesn't experiences only the desired DC component. But to reduce the ripple level below acceptable level, i.e. below 5% at least a capacitor rated at 0.8F is required. For purpose of simulation, a 1A DC current source was connected in parallel to 2A 60Hz current source and 1A 120Hz current source to recreate waveform similar to that observed on DC side of the MMC submodule. The capacitor value was gradually increased from 500mF till the ripple value was reduced to less than 5%.

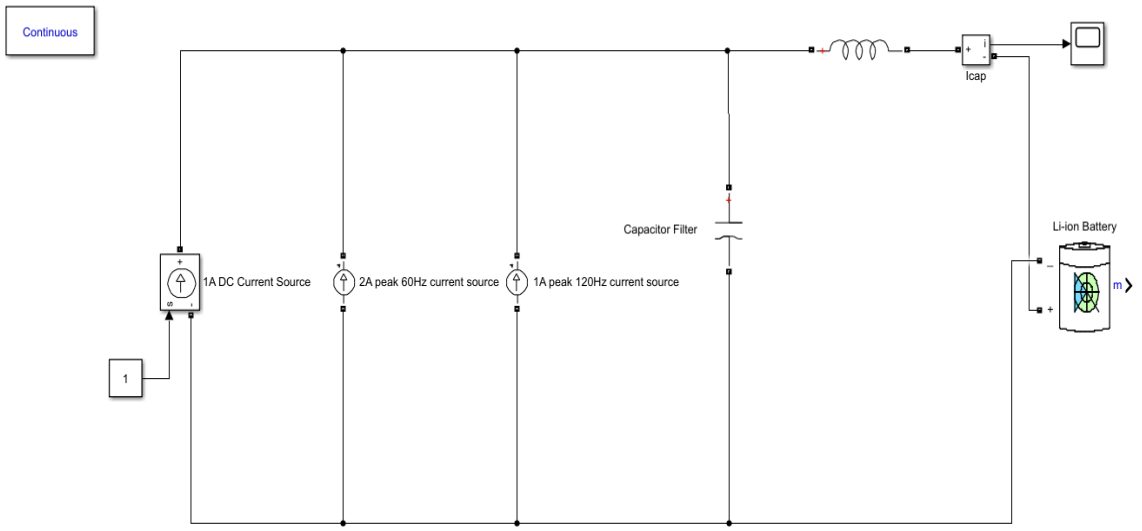


Figure 22. Matlab filter simulation model

The dimensions of a 1F electrolytic capacitor is 10cm in diameter and 25cm in length. This is quite large volume. Hence proper design considerations need to be taken in order to incorporate capacitor within the submodule of MMC.

One solution to this could be implementing a super capacitor in place of electrolytic capacitor. Fig 23. And Fig. 24 show the Fast Fourier Analysis of the current waveform at the battery terminals using 0.8F capacitor and 0.8F ultra capacitor respectively.

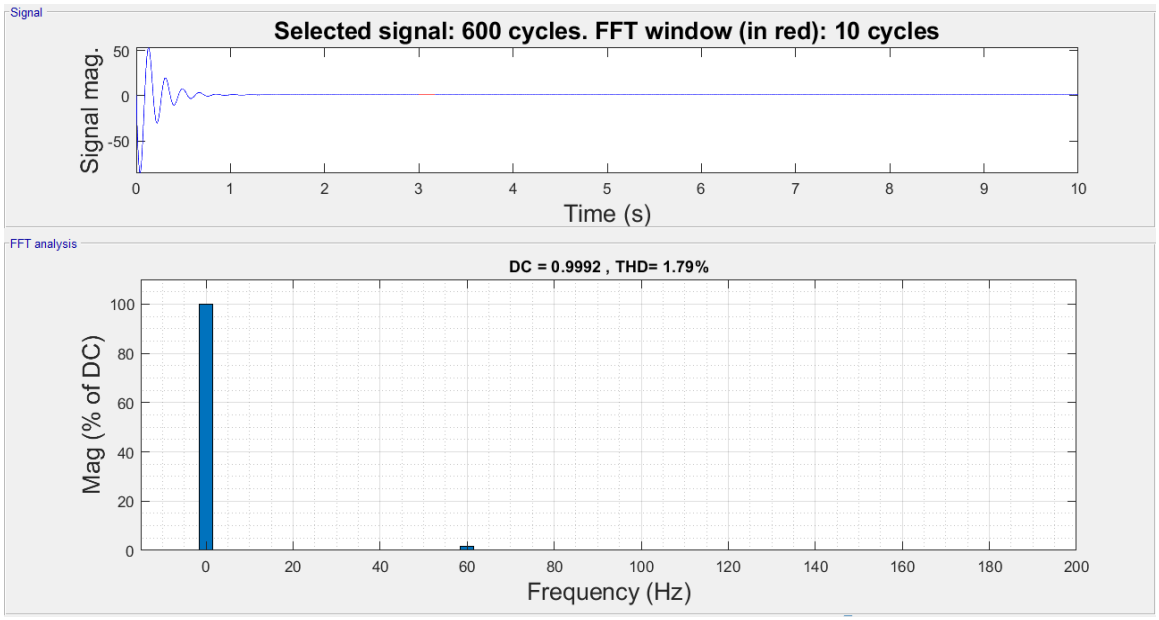


Figure 23 Reduction in ripple due to 0.8F capacitor

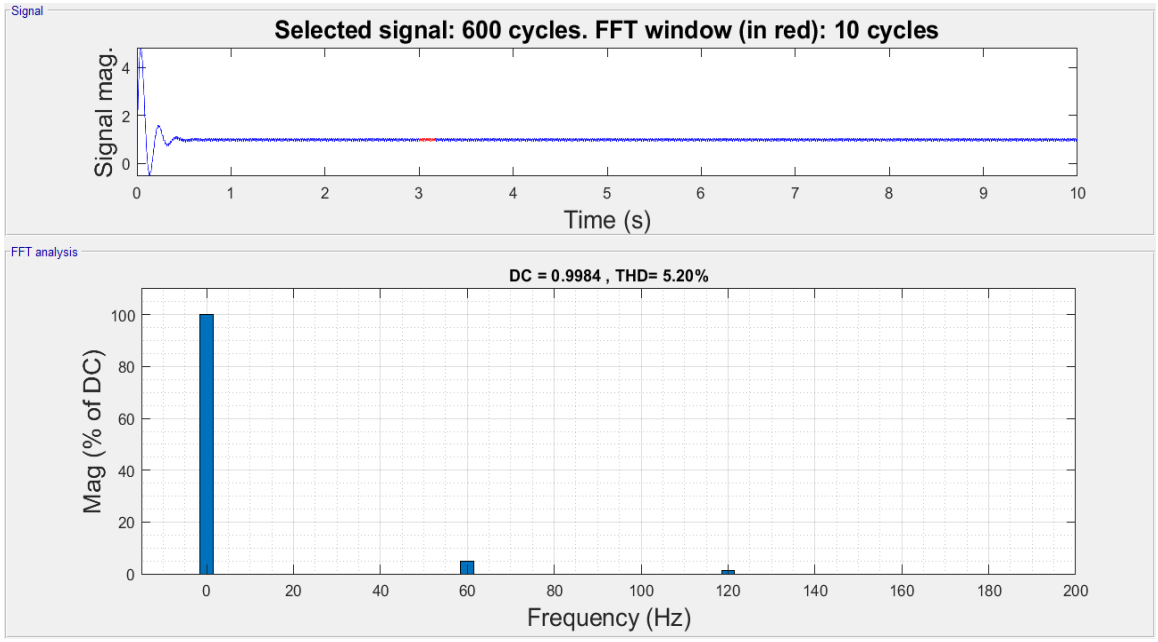


Figure 24 Reduction in ripple due to 0.8F ultra-capacitor

A trade-off can be made in the cost and size by installing a capacitor and ultra-capacitor in series. The same has been simulated in MATLAB environment. The effect has been illustrated in Fig. 25 and Fig. 26.

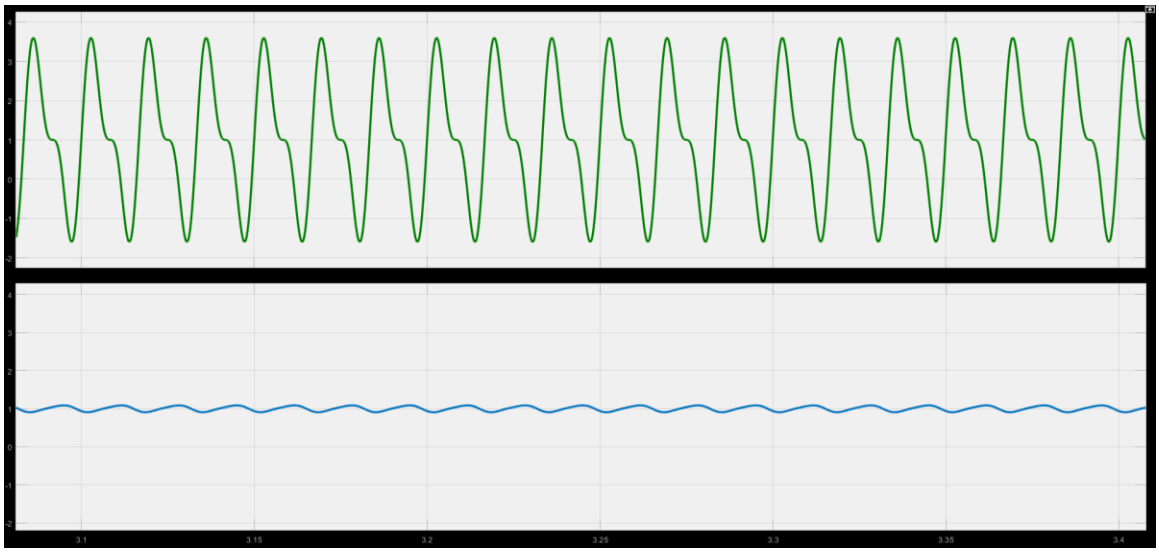

Figure 25. Attenuation obtained using series capacitor and ultra capacitor combination

For simulation purposes the capacitor and ultra-capacitor capacitances were equally selected to be 0.4 F each such that the total capacitance of series combination is 0.8F same as earlier configurations. This combination is less effective than individually installed components as the same capacitance reduces the ripple content just below 9%. But giving more design considerations, the solution can be implemented making trade-off between size and cost of passive filter.

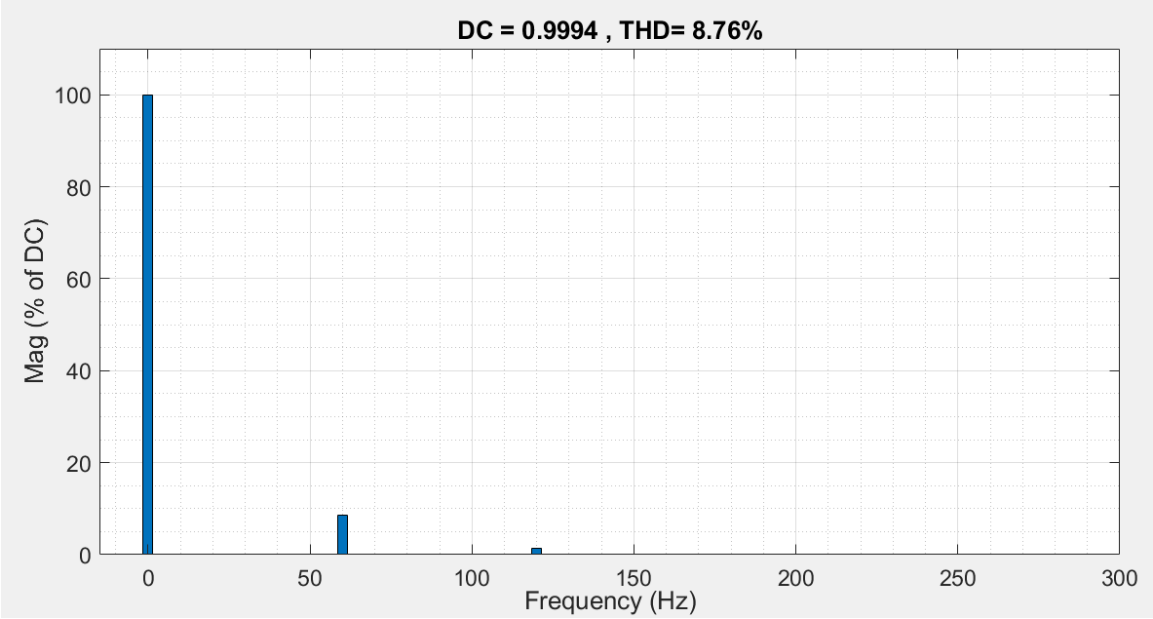


Figure 26. Fast fourier analysis of waveform in figure 25

# XIII. ACTIVE FILTERING

## A. Shunt Active Filter

The pulsating power caused by presence of large amount of ripple calls for large passive components like the capacitor. Besides, it is the reason for additional converter losses thus reducing the operating efficiency and also can cause malfunction of controller. Many studies have been done and various solutions to reduce the DC link ripple have been proposed. The principle of active filtering is to inject equal and opposite waveform to that of the ripple. The buffer circuit used to absorb the ripple content is generally placed in parallel with the DC link, the battery in this case. Main reason behind it being, parallel buffers being more efficient than series buffers as only ripple energy is processed by them instead of entire supply energy as in series buffers. Also, majority buffer circuits select capacitors as ripple energy storage element rather than inductors. The reason being that capacitors have higher energy density than inductors, lower losses and smaller size.

Figure 27 shows the block diagram for active filter. Active Power Filters (APF) are used to provide dynamic compensation to the system. They continuously sample the system waveform and compare it with the reference waveform which is a constant DC and provide compensation so as to minimize the error. Shunt APF are voltage source inverters which act as a current source. They are implemented primarily for mitigation of current harmonics. Shunt APF generates currents which is equivalent to the ripple component of the load current but is of opposite phase and injects it into the power system thus cancelling the ripple component. Shunt APF employs an IGBT based inverter system

which can operate at a high switching frequency to generate harmonic equivalent currents with high accuracy. The inverter is powered by a DC source generally a capacitor bank.

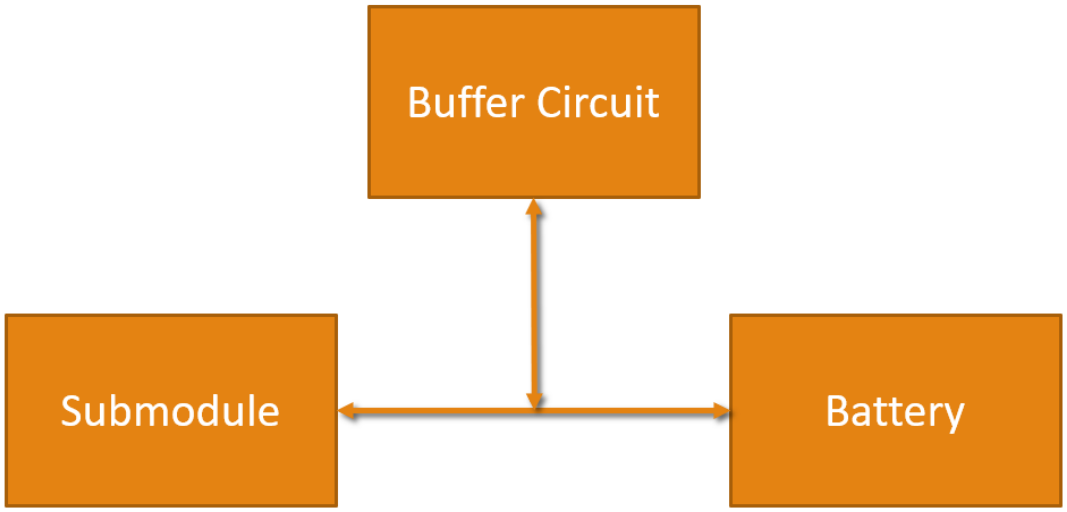


Figure 27 Active filtering using buffer circuit

The buffer circuit being a H-bridge or a full bridge converter and incorporates very complicated control strategy and hence is extremely costly solution.

B. Interlinking Buck-Boost Converter

A bidirectional DC-DC buck boost converter is used to link the battery unit with the submodule. This topology can smooth the power fluctuations by implementing ripple control using the interlinking converter and also improve voltage of the DC-link as the variations in battery voltage during its operation are compensated by the boost action of the converter. Besides this topology can implement voltage and current control of battery charging and discharging profiles thus ensuring better usage of battery units as discussed

in Battery Management System Section. The buck boost converter is a half bridge unit and hence a more economical solution compared to the shunt active power filter but since the interlinking unit is in series, the energy transfer efficiency is slightly affected between the battery and submodules. Fig. 28 illustrates the submodule for proposed topology.

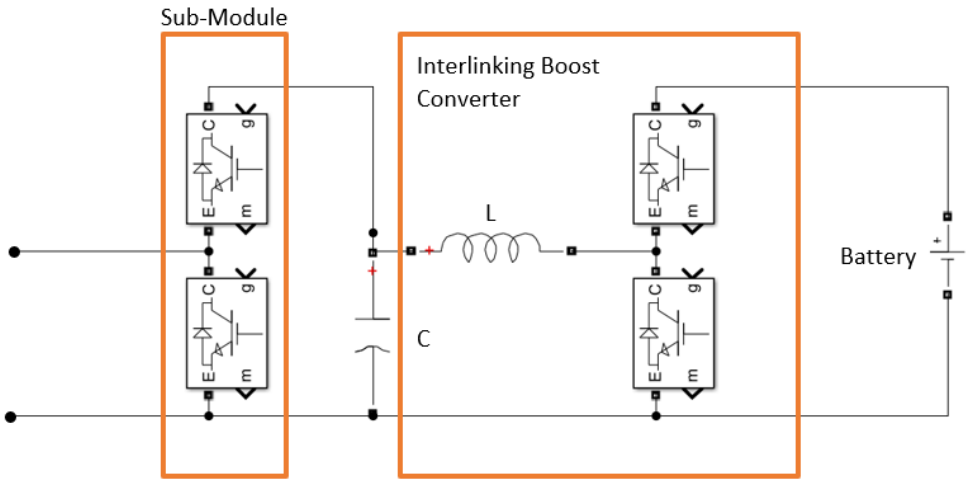


Figure 28. Interlinking boost converter

# XIV. CONCLUSION

BESS integrated into MMC has been proposed in many papers so far. But as per the experimental results, this implementation has negative effect on the battery performance and lifetime. The low frequency ripple observed by the battery during charging and discharging process causes accelerated degradation of battery which will lead to drastic reduction in life time of the battery. Hence more consideration needs to be done regarding filter design on the DC side of the MMC submodules.

# REFERENCES


1. Ota, J. I. Y., Sato, T., & Akagi, H. (2016). Enhancement of performance, availability, and flexibility of a battery energy storage system based on a modular multilevel cascaded converter (MMCC-SSBC). *IEEE Transactions on Power Electronics*, *31*(4), 2791-2799.

2. Vasiladiotis, M., & Rufer, A. (2015). Analysis and control of modular multilevel converters with integrated battery energy storage. *IEEE Transactions on Power Electronics*, *30*(1), 163-175.

3. Zhang, L., Gao, F., Li, N., Zhang, Q., & Wang, C. (2015, September). Interlinking modular multilevel converter of hybrid AC-DC distribution system with integrated battery energy storage. In *Energy Conversion Congress and Exposition (ECCE), 2015 IEEE* (pp. 70-77). IEEE.

4. He, H., Xiong, R., & Fan, J. (2011). Evaluation of lithium-ion battery equivalent circuit models for state of charge estimation by an experimental approach. *energies*, *4*(4), 582-598.

5. Abu-Sharkh, S., & Doerffel, D. (2004). Rapid test and non-linear model characterisation of solid-state lithium-ion batteries. *Journal of Power Sources*, *130*(1-2), 266-274.

6. Haifeng, D., Xuezhe, W., & Zechang, S. (2009, September). A new SOH prediction concept for the power lithium-ion battery used on HEVs. In *Vehicle Power and Propulsion Conference, 2009. VPPC'09. IEEE* (pp. 1649-1653). IEEE.

7. Chen, M., & Rincon-Mora, G. A. (2006). Accurate electrical battery model capable of predicting runtime and IV performance. *IEEE transactions on energy conversion*, *21*(2), 504-511.

8. Zhang, L., Gao, F., & Li, N. (2016). Control strategy of MMC battery energy storage system under asymmetrical grid voltage condition. *Chinese Journal of Electrical Engineering*, *2*(2), 76-83.

9. Bergveld, H. J., Kruijt, W. S., & Notten, P. H. (2011). *Battery management systems: Design by modelling*. Dordrecht: Springer.

10. Welcome to Battery University! Retrieved March 25, 2018, from http://www.batteryuniversity.com/

11. Purwadi, A., Rizqiawan, A., Kevin, A., & Heryana, N. (2014, December). State of charge estimation method for lithium battery using combination of coulomb counting and adaptive system with considering the effect of temperature. In *Power Engineering and Renewable Energy (ICPERE), 2014 International Conference on* (pp. 91-95). IEEE.

12. Vitorino, M. A., Alves, L. F. S., Wang, R., & de Rossiter Corrêa, M. B. (2017). Low-frequency power decoupling in single-phase applications: A comprehensive overview. *IEEE Transactions on Power Electronics*, *32*(4), 2892-2912.

# APPENDIX

## A. PANASONIC NCR18650 CELL DATASHEET

Panasonic
ideas for life

# NCR-18650B

## LITHIUM-ION / NNP + HRL TECHNOLOGY

A perfect combination of high energy density (e.g. NNP technology), safety (e.g. PSS and HRL technology) and long-life shows what is possible with Lithium-Ion battery technology from Panasonic. Excellent battery safety on one hand, and superior battery performance on the other: this is what Panasonic stands for.

### LI-ION • 3D ILLUSTRATION

1 Positive pole
2 Positive Temperature Coefficient Device (PTC)
3 Gasket
4 Collector
5 Insulator
6 Cathode
7 Anode
8 Negative pole (cell can)
9 Separator
10 Current Interrupt Device (CID)
11 Exhaust gas hole



### Nickel Oxide Based New Platform (NNP)

This new Lithium-Ion battery technology contains on one side a unique high capacity Nickel based positive electrode and on the other side a material and processing technology. The latter prevents deformation of the Alloy-based negative electrode when subjected to repeated charge and discharge. This is what our **Nickel Oxide Based New Platform (NNP)** stands for.*1

**Characteristics of the Panasonic NNP technology:**

- Good cycle life performance
- High energy density
- The new Nickel positive electrode excels in durability in actual use and charge retention
- Low self-discharge
- Long storage reliability through reduced metal elution

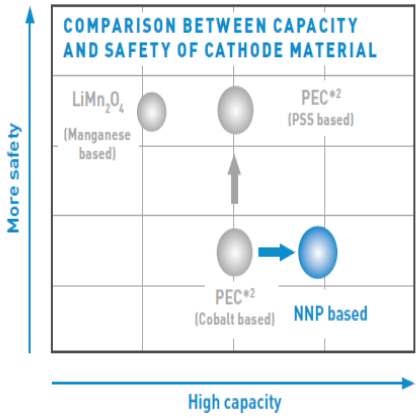

## Heat Resistance Layer (HRL)

Nowadays all electronic devices getting more powerful, sophisticated and feature-laden and therefore require more robust and safer batteries. Increasing energy-density, however, raises the risk of overheating and ignition due to internal short-circuiting. Panasonic deploys the **Heat Resistance Layer (HRL)** technology to improve the safety of Lithium-Ion batteries significantly. This heat resistance layer consists of an insulating metal oxide on the surface of the electrodes which prevents the battery from overheating if an internal short-circuit occurs.

**Safety is the base for everything. Higher energy can be established based on safety technology.**

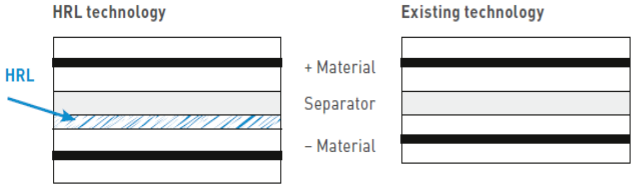


*1 Panasonic Lithium-Ion cells must always be equipped with a safety unit.
*2 PEC: Panasonic Energy Company.

Panasonic BATTERIES
Quality is our Business.

# NCR-18650B

## LITHIUM-ION / NNP + HRL TECHNOLOGY

DIMENSIONS (MM)


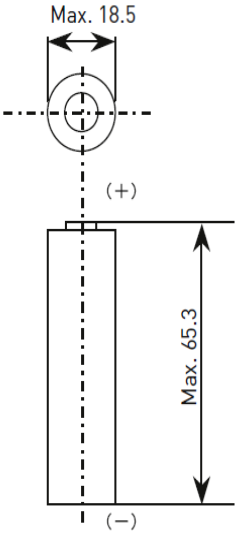


TYPICAL DISCHARGE CHARACTERISTICS

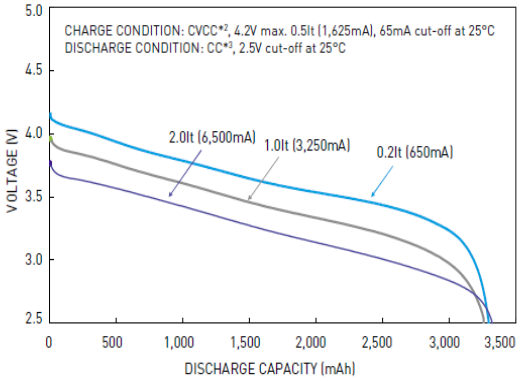


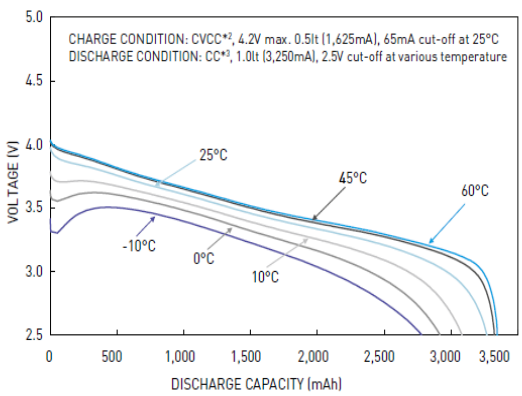


SPECIFICATIONS

| Model number | NCR-18650B |
|---|---|
| Nominal voltage (V) | 3.6 |
| Nominal capacity*1 - Minimum (mAh) | 3,250 |
| Nominal capacity*1 - Typical (mAh) | 3,350 |
| Dimensions - Diameter (mm) | 18.5 |
| Dimensions - Height (mm) | 65.3 |
| Approx. w^eight (g) | 47.5 |

## TYPICAL CHARGE CHARACTERISTICS

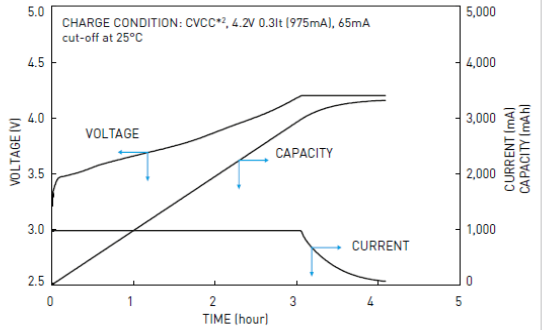


## TYPICAL CYCLE CHARACTERISTICS

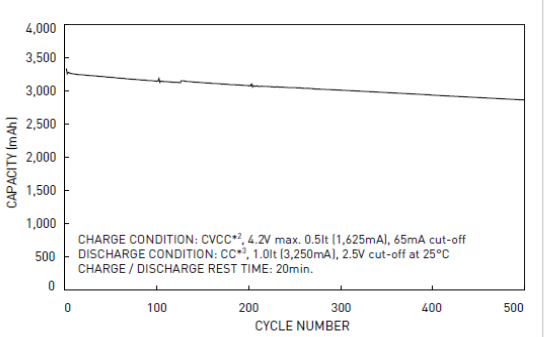


*1 Charge: Constant Voltage / Constant Current, 4.2V, max. 1,625mA, 65mA cut-off; Discharge: Constant Current, 650mA, 2.5V cut-off; Temperature: 25°C
*2 CVCC: Constant Voltage / Constant Current *3 CC: Constant Current

**Notice to Readers**

We are unable to support single cell business or accept orders from consumers. We design Lithium-Ion battery packs including a suitable safety unit device based on the technical specification of the customer. Due to the need for careful review when selecting Lithium-Ion battery solutions please contact your local Panasonic Sales Office. In order to avoid a lack of supply please check the battery availability with your Panasonic sales team before design-in.

Panasonic

Panasonic Industrial Devices Sales Europe I Winsbergring 15 I 22525 Hamburg I Website: http://industrial.panasonic.com/eu

## Cell Type NCR18650B

### Specifications

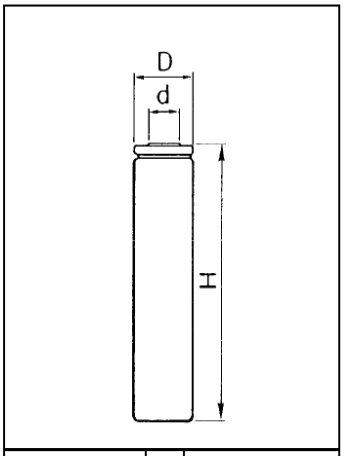


| Dimensions(Typ.) of Bare Cell | | |
|---|---|---|
| | H | 64.93mm |
| | D | 18.2mm |
| | d | 7.9mm |

Discharged State after Assembling

| | | |
|---|---|---|
| Rated Capacity (at 20℃) | | Min.3200mAh |
| Nominal Capacity (at 25℃) | | Min.3250mAh<br>Typ.3350mAh |
| Nominal Voltage | | 3.6V |
| Charging Method | | Constant Current -Constant Voltage |
| Charging Voltage | | 4.2V |
| Charging Current | | Std.1625mA |
| Charging Time | | 4.0hrs. |
| Ambient Temperature | Charge | +10～+45℃ |
| | Discharge | -20～+60℃ |
| | Storage | -20～+50℃ |
| Weight (Max.) | | 47.5g |
| Dimensions (Max.)<br>Maximum size without tube | (D) | 18.25mm |
| | (H) | 65.10mm |
| Volumetric Energy Density | | 676Wh/l |
| Gravimetric Energy Density | | 243Wh/kg |



Lithium ion
Rechargeable battery

## Discharge Rate Characteristics for NCR18650B

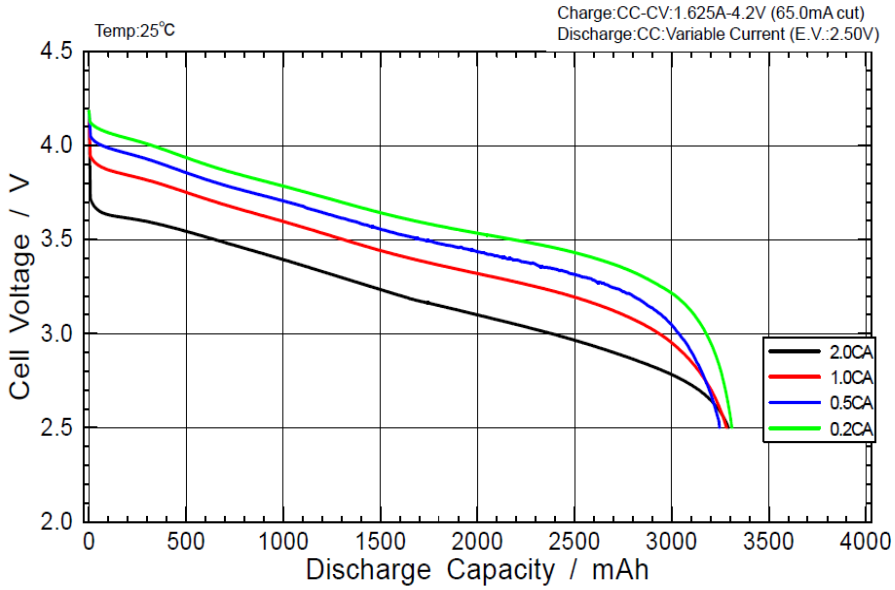


2G23X0KYKU
Panasonic ideas for life

## Discharge Temperature Characteristics for NCR18650B

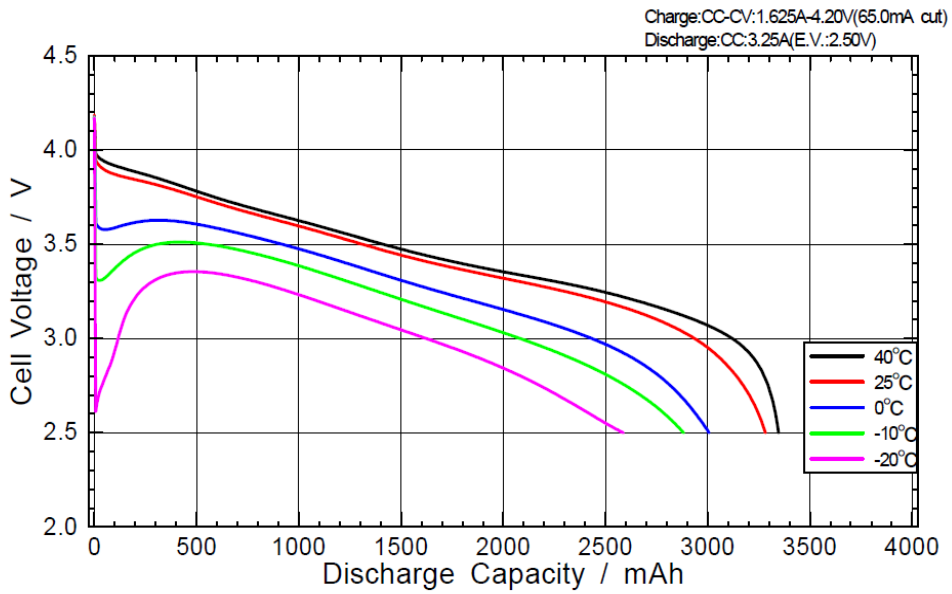






## Charge Characteristics for NCR18650B

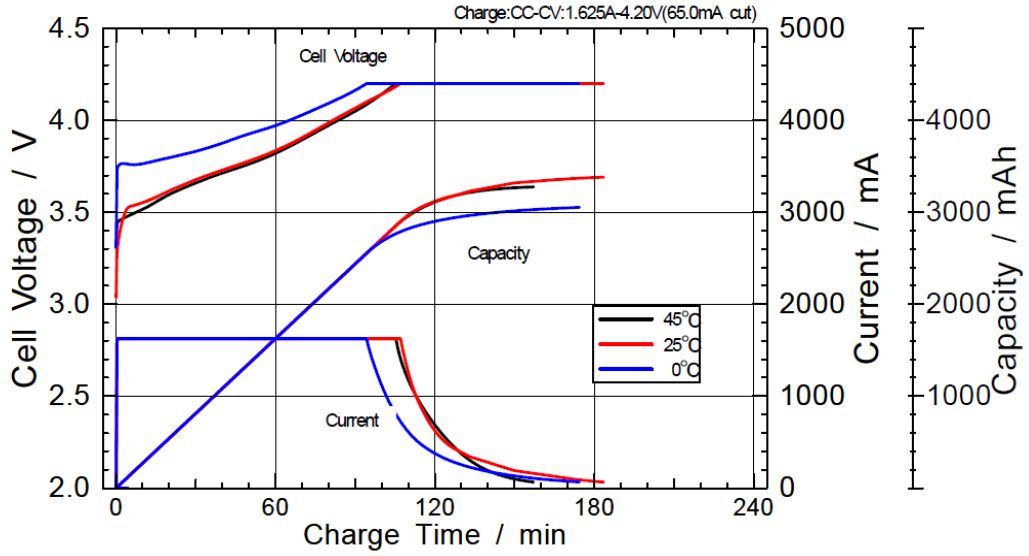

# APPENDIX

## B. DATA COLLECTED SUMMER2017-SPRING2018

For all Tables Rnew = Average ohmic resistance of new cell calculated for SoC 20% through 90%

R = Average ohmic resistance of cell calculated for SoC 20% through 90% after testing Regime.

Reol = End of life resistance of cell which is 1.6xRnew.

SoH = state of health of cell.

A. Resistance Recorded for 0% current Ripple

| Rnew | R | Reol | SoH(%) |
|---|---|---|---|
| 0.22996167 | 0.23573333 | 0.36793867 | 0.95816936 |

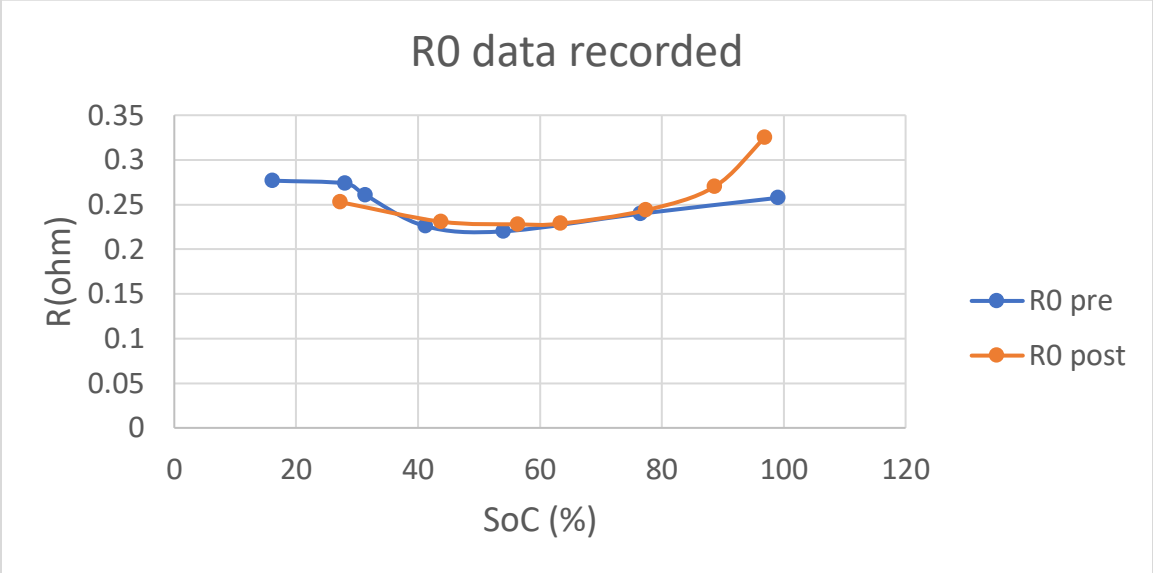

B. Resistance Recorded for 5% ripple content

| Rnew | R | Reol | SoH |
|---|---|---|---|
| 0.093 | 0.09677 | 0.1488 | 0.932437 |

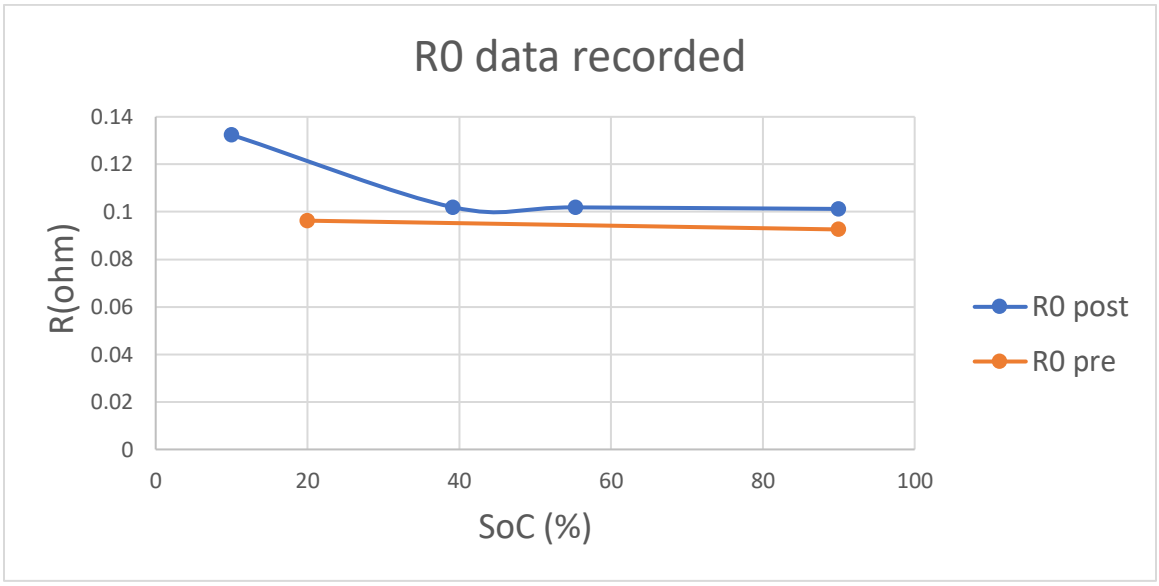


C. Resistance Recorded for 10% ripple content

| Rnew | R | Reol | SoH |
|---|---|---|---|
| 0.1758 | 0.20715 | 0.28128 | 0.702787 |

D. Resistance recorded for 20% ripple content

| Rnew | R | Reol | SoH |
|---|---|---|---|
| 0.10535 | 0.125625 | 0.16856 | 0.679244 |

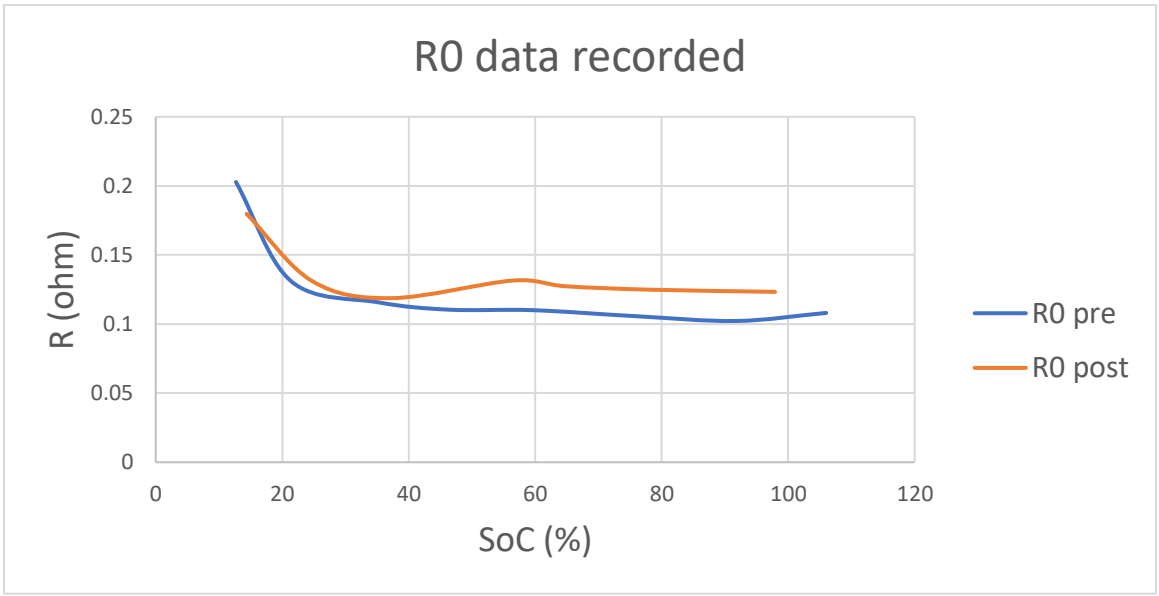


E. Resistance recorded for MMC dc side waveform

| R | Rnew | Reol | SoH |
|---|---|---|---|
| 0.105285 | 0.08155 | 0.13776 | 0.577744 |